Journal Pre-proof

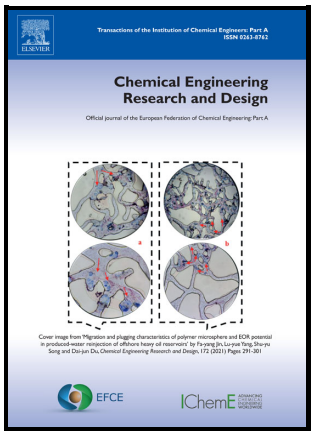

Hydrodynamics and gas-liquid mass transfer in an oscillatory flow reactor: influence of liquid properties

F. Almeida, F. Rocha, J.A. Teixeira, A. Ferreira

PII: S0263-8762(23)00177-6

DOI: https://doi.org/10.1016/j.cherd.2023.03.030

Reference: CHERD5516

To appear in: *Chemical Engineering Research and Design*

Received date: 8 December 2022
Revised date: 15 March 2023
Accepted date: 15 March 2023

Please cite this article as: F. Almeida, F. Rocha, J.A. Teixeira and A. Ferreira, Hydrodynamics and gas-liquid mass transfer in an oscillatory flow reactor: influence of liquid properties, *Chemical Engineering Research and Design,* (2023) doi:https://doi.org/10.1016/j.cherd.2023.03.030

Hydrodynamics and gas-liquid mass transfer in an oscillatory flow reactor: influence of liquid properties

F. Almeida[1,2], F. Rocha[1,2], J. A. Teixeira[3,4] and A. Ferreira[1,2*]

*Corresponding author: antonio@fe.up.pt

[1]LEPABE - Laboratory for Process Engineering, Environment, Biotechnology and Energy, Faculty of Engineering, University of Porto, Rua Dr. Roberto Frias, 4200-465 Porto, Portugal

[2]ALiCE - Associate Laboratory in Chemical Engineering, Faculty of Engineering, University of Porto, Rua Dr. Roberto Frias, 4200-465 Porto, Portugal

[3]CEB - Centre of Biological Engineering, University of Minho, 4710-057 Braga, Portugal

[4]LABBELS - Associate Laboratory in Biotechnology, Bioengineering and Microelectromechanical Systems, Faculty of Engineering, University of Minho, Rua da Universidade, 4710-057, Braga, Portugal

Highlights

- Mass transfer in the OFR-SPC was higher than in the conventional gas-liquid contactors, with moderate power consumption.
- An increase in oscillatory conditions improves mass transfer.
- For viscous medium, an oscillation increase originates a modal BSD, compared to bubble column.
- Higher oscillations decrease k_L in the presence of ethanol, in opposite to sucrose solutions.
- The addition of ethanol or sucrose barely affected gas holdup in the OFR-SPC face to common gas-liquid contactors.

Abstract

Liquid properties, such as, surface tension and viscosity are important parameters as they control gas-liquid mass transfer in bioprocesses. An oscillatory flow reactor provided with smooth periodic constrictions (OFR-SPC) was considered to evaluate its potential for mass transfer performance in non-pure gas-liquid systems. The effect of surface tension and viscosity on the volumetric ($k_L a$) and liquid-

side mass transfer coefficients (k_L), interfacial area, (a), gas holdup (ε_G) and bubbles' dynamics were investigated under different operational conditions (oscillation amplitude (x_0) and frequency (f) and superficial gas velocity (u_g)). Two liquid phases, ethanol and sucrose aqueous solutions covering a range of surface tension and viscosity values were used. For the bubble size distribution (BSD) measurements an image analysis technique was used. A Design of Experiment (DoE) methodology was implemented in this work to establish the relation of x_0, f, u_g, surface tension and viscosity with $k_L a$. According to the results, changes in the liquid properties and operational conditions showed marked effects on bubble's size and mass transfer. However, surface tension and viscosity had no significant influence on ε_G, contrary to the reported for common contactors, where ε_G increased in the presence of ethanol and decreased at moderate/high viscosities. Moreover, it was found that increasing the oscillatory movement notably improved k_L, and $k_L a$ (2 to 6-fold), either in ethanol or sucrose solutions, compared to common reactors, even with moderate power consumption (~ 105 W m^{-3}). This improvement resulted from the bubbles' breakage, which originates bubbles with small and approximately the same size (homogeneous regime) enhancing a, instead, lower oscillations resulted in large bubbles (heterogeneous regime). The results demonstrate that the OFR-SPC can ensure outstanding mass transfer rates, with potential and feasibility for use in gas-liquid bioprocesses, where mass transfer and liquid properties are important.

Keywords: Oscillatory flow reactor; Gas-liquid mass transfer; Gas holdup; Sauter mean diameter; Design of experiments (DoE); Multiphase reactors.

Graphical abstract

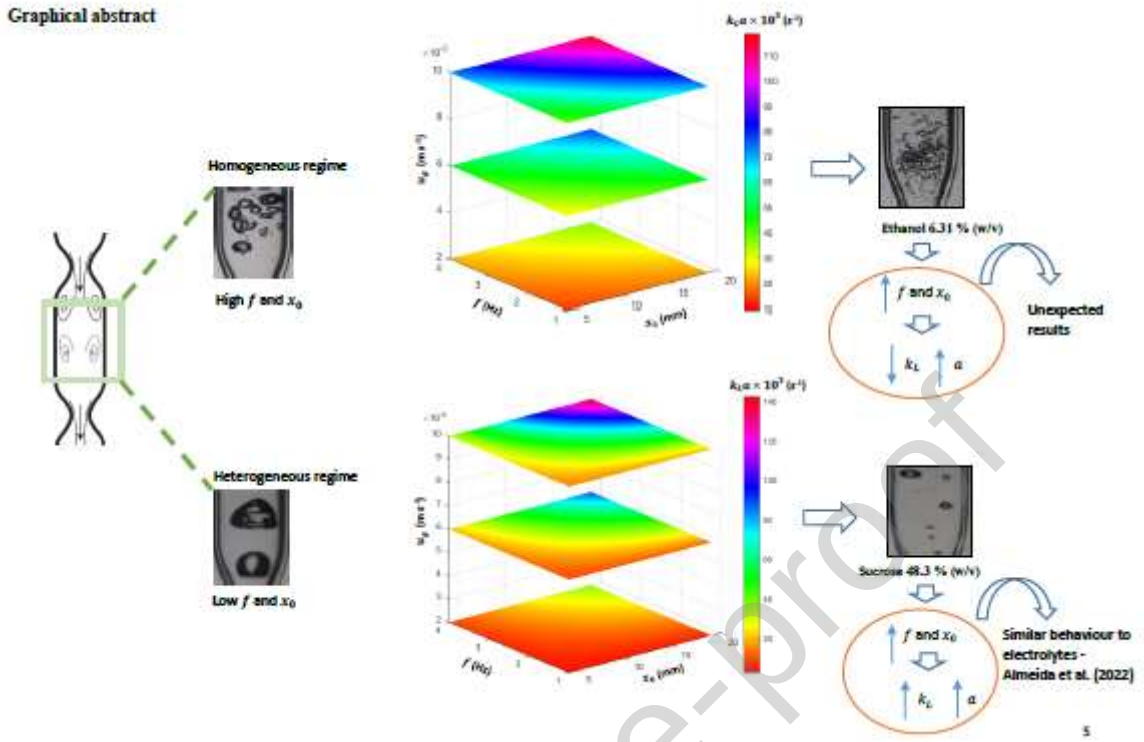

1. Introduction

Gas-liquid mass transfer is a major operation in chemical or biochemical industrial processes. Generally, in gas-liquid processes, bubbles are sparged into the liquid, which rise along the reactor promoting complex gas-liquid interactions. During the bubble rise, surface tension and viscosity forces act on the bubble, controlling its size, surface mobility, and, more important its rise velocity, since it defines the bubble residence time, thus, the gas-liquid mass transfer (Basařová et al., 2018). Mass transfer between a bubble and the surrounding liquid relies on the surface mobility, which is affected by the presence of compounds in the liquid phase.

The volumetric liquid-side mass transfer coefficient ($k_L a$) is typically used to characterize the mass transfer. However, for a better understanding of the mass transfer process it is important to study the individual parameters, liquid-side mass transfer coefficient (k_L) and specific interfacial area (a). In turn, bubble size and gas holdup (ε_G) are crucial parameters as they determine the gas-liquid interfacial area, available for mass transfer (Mouza et al., 2005). Bubble size distribution (BSD) and ε_G greatly depend on the reactor geometry, gas sparger, operating conditions and liquid properties, namely surface tension and viscosity (Mouza et al., 2005).

The effect of the liquid surface tension and viscosity on the hydrodynamics and mass transfer have been thoroughly investigated either in bubble columns (BCs) (Chaumat et al., 2007; Ferreira et al., 2012) or in airlift reactors (Al Ezzi and Najmuldeena, 2014; Molina et al., 1999; Onken and Weiland, 1980). Surface tension has been extensively studied in alcohol solutions. Alcohol is an amphiphilic

molecule, with hydrophilic/hydrophobic characteristics, adsorbed at the gas-liquid interface. It is known that alcohol addition reduces the surface tension and the probability of bubble coalescence. This behaviour increases the interfacial area between gas and liquid, and decreases bubble rise velocity, therefore, improving ε_G and mass transfer performance (Albijanić et al., 2007; Chaumat et al., 2007; Hebrard et al., 2009; Hur et al., 2014). Also, Ferreira et al. (2012) in a BC demonstrated that ethanol reduces the surface tension, favouring the formation of small bubbles by breakage and inhibiting coalescence, thus, increasing a and, hence, the $k_L a$. Mouza et al. (2005) operating a BC and using fine pore spargers found that the decrease in surface tension reduced the Sauter mean bubble diameter (d_{32}) and barely increased ε_G. The effect of ethanol on ε_G and flow regime was also investigated by Krishna et al. (2000) under elevated pressure. The authors claimed that ethanol increased ε_G due to a delay in the regime transition point from homogeneous to heterogeneous, result of the coalescence suppression. Elevated pressure enhanced the ε_G and stabilized the homogeneous regime.

In the study performed by Onken and Weiland (1980) the authors compared ε_G results in an airlift and those from BCs. In airlift alcohols barely affected ε_G, whereas in BCs ε_G increased more than 2-fold. The authors concluded that the lower ε_G in the airlift was due to the bubble coalescence inhibition and mainly due to the high liquid circulation velocity. The liquid circulation leads to the acceleration of the rising bubbles in the upward liquid flow, in opposite to BC operation, i.e., without circulation. Lower ε_G combined with uniform BSD greatly prevents bubble's swarm (Onken and Weiland, 1980). According to the authors, this huge difference in the ε_G behaviour between these two types of reactors was reflected in $k_L a$ values, i.e., in airlift $k_L a$ increased 2-fold and in BC enhanced 6-fold. This behaviour means that airlift requires higher aeration rates and heights. Recently, Ramezani et al. (2017) also reported a decrease in surface tension in the presence of ethanol when using a multiphase Taylor-Couette vortex bioreactor. This decrease demotes bubble coalescence, resulting in smaller bubbles and higher a and $k_L a$ values, however, for higher ethanol concentrations the authors found a minor increase.

Liquid viscosity has been extensively studied in gas-liquid mass transfer. Typically, the increase in liquid viscosity leads to a decrease of turbulence of the liquid phase, favouring the formation of large bubbles by coalescence, increasing d_{32} (Mouza et al., 2005). Studies of Ferreira et al. (2012) in a BC demonstrate that the viscosity increase affects both individual parameters of $k_L a$, i.e., significant increase of a and decrease of k_L was observed. According to Martin et al. (2007) the liquid viscosity has a dual effect on the bubble's hydrodynamics, the delay in the bubble expansion, and in the molecular movement at the bubble's surface, both contributing to reduction in $k_L a$. This effect is consistent with previous observations reported by Onken and Weiland (1980).

Although BC and airlift reactors have been widely used in industry to improve the mass transfer of gas-liquid systems, back mixing, insufficient and nonuniform mixing are still problems often reported (Ahmed et al., 2018). To avoid those problems and to enhance the mass transfer, researchers have focused either on optimizing operational conditions or on improving devices: (i) gas spargers (Besagni and Inzoli, 2019); (ii) static mixers (Chisti et al., 1990); (iii) sieve plates (Luo et al., 2013); (iv)

oscillatory flow reactor (OFR) designs. The oscillatory technology has also been optimized through baffles designs whether single orifice (Oliveira and Ni, 2004, 2001), multi-orifice (Ahmed et al., 2019, 2018), smooth periodic constrictions (SPC) (Almeida et al., 2022; Ferreira et al., 2017; Reis et al., 2008, 2007), 2D SPC (Almeida et al., 2018; Cruz et al., 2019; P. Cruz et al., 2021a, 2021b; P. C. Cruz et al., 2021) or with helical, central and integral baffles (Ahmed et al., 2018)).

Despite the extensive studies on the OFR performance there is a gap regarding the influence of non-pure systems on gas-liquid mass transfer. For example, the effect of liquid properties on the hydrodynamics and mass transfer characteristics and particularly on the individual parameters k_L and a remain unexplored. Moreover, gas-liquid industrial processes rarely use only water, instead, impure systems are commonly used. In this study an oscillatory flow reactor provided with smooth periodic constrictions (OFR-SPC), designed according to EP3057694 (B1) patent, was considered to investigate the mass transfer in a non-pure gas-liquid system. It consists of a glass tube containing periodically SPC, equally spaced, operating under oscillatory flow mixing (OFM) controlled by oscillation amplitude (x_0) and frequency (f) imposed on the liquid by means a diaphragm, originating the formation/dissipation of eddies inside each SPC and their propagation in radial and axial directions. Therefore, the liquid moves from the walls toward the centre of the reactor promoting the efficiency of the mixing. This phenomenon promotes a decrease in bubble size and an increase in gas holdup, hereby increasing the volumetric liquid-side mass transfer coefficient ($k_L a$), specific interfacial area (a) and liquid-side mass transfer coefficient (k_L) (Almeida et al., 2022; Gonçalves et al., 2021; Ferreira et al., 2015; Reis et al., 2008, 2007). For exemple, Ferreira et al. (2015) sustain their observation - a $k_L a$ increase up to 10 times was observed in an OFR-SPC in comparison with a BC - based on the bubble size obtained (< 3 mm). According to the authors small bubbles (< 3 mm) suffer more influence of the hydrodynamic conditions, being trapped inside the vortices, leading to an increase in the renewal rate of the liquid film at the interface and by this way to a k_L increase.

Therefore, this work aimed to evaluate the potential of the OFR-SPC, designed according to the EP3057694 (B1) patent, for gas-liquid mass transfer, in a non-pure system. The influence of liquid properties, including surface tension and viscosity, on the hydrodynamics (ε_G, BSD, liquid velocity and bubble rise velocity) and individual k_L and a values were evaluated, under different operational conditions.

2. Materials and Methods

2.1. Experimental setup and operating conditions

The experiments were carried out in an oscillatory flow reactor provided with smooth periodic constrictions (OFR-SPC) schematically represented in Fig. 1. It presents an inner diameter of 0.016 m providing a total volume of 7×10^{-5} m^3. The initial height of the liquid was set at 0.45 m. The SPC dimensions are not presented, these are protected by the W0/2015/056156 patent.

[Figure 1 here]

The OFR-SPC is a reactor able to operate in a vertical or horizontal position, in batch or continuous mode. In the present work, all the experiments were performed in a vertical orientation and semi-batch mode operation (continuous gas phase and batch liquid phase), at 298.15 K and pressure of 1.013×10^5 Pa. The temperature was maintained through a circulating thermostatic bath (Tectron Bio, JP Selecta) connected to a water jacket fitted around the tube. A rotational motor (Cat, R100 C) was attached at the tube by a piston and a diaphragm to oscillate the liquid, providing a sinusoidal oscillation, according to a set of oscillatory conditions (oscillation amplitude (x_0) and frequency (f)) detailed in Table 1. The oscillatory flow was characterized by dimensionless numbers, oscillatory Reynolds number (Re_o) and Strouhal number (St). The Re_o describes the intensity of mixing applied in the reactor and it is defined by Equation 1:

$$\mathrm{Re_o} = \frac{2\pi f x_0 \rho D}{\mu} \tag{1}$$

The St describes the eddy propagation inside the baffles' cavity and it is defined by Equation 2:

$$\mathrm{St} = \frac{D}{4\pi x_0} \tag{2}$$

Where ρ represents the density (kg m^{-3}), μ the dynamic viscosity (kg m^{-1} s^{-1}), x_0 the oscillation amplitude (m) and f the frequency (Hz) of the liquid, and D (m) the inner diameter of the straight section.

Table 1 details the experimental operational conditions evaluated in this study: (i) oscillation amplitude (4×10^{-3} to 1.9×10^{-2} m); (ii) oscillation frequency (1 to 4 Hz); (iii) superficial gas velocity (u_g) (4.9×10^{-4} to 9.8×10^{-3} m s^{-1}).

[Table 1 here]

Air K (reconstituted air, 20% of O_2 and 80% of N_2) was used as gas phase. Gas flow rates ranged from 8.33×10^{-8} to 1.66×10^{-6} m^3 s^{-1} (detailed in Table 1) and they were controlled by a precision gas mass flow controller (Alicat Scientific). The superficial gas velocity was calculated from the gas flow rate which in turn was divided by the area of the reactor tube. The diameter used to calculate this area was the hydraulic diameter (d_h): $d_h = D \times 0.4/0.44$. Aqueous solutions, 6.31 % (w/v) (1.37 M) of ethanol (Sigma Aldrich, 99 (v/v) %) and 48.3 % (w/v) (1.41 M) of sucrose (RAR, 99 % purity) were used as liquid phases. Distilled water was used as liquid phase for $k_L a$ control experiments. Table 2 details the surface tension and viscosity values of the solutions evaluated at 298.15 K.

[Table 2 here]

2.2. Mass transfer experiments – methodology

Two independent sets (ethanol and sucrose solutions (Table 2)) of mass transfer experiments were conducted in the OFR-SPC according to the operating conditions defined in Table 1. The $k_L a$ was determined using a dynamic method performed as follows. Firstly, before each experiment, the liquid

was deoxygenated by injecting nitrogen at the bottom of the OFR-SPC (stripping process) until the dissolved oxygen concentration reaches nearly 0 mg l^{-1}. At this point, air is fed into the OFR-SPC by a needle with an inner diameter of 0.3 mm. The dissolved oxygen concentration in the liquid was continuously measured at the top of the OFR-SPC, using a fibreoptic oxygen meter (OXR50-HS, Pyroscience) connected to the FireSting O_2 instrument (Pyroscience). The dissolved oxygen concentration was recorded over the time in a computer through the FireSting Logger software for further analysis. To ensure that the concentration is homogeneous across the reactor, the concentration was measured at the top and at the bottom, which revealed to be similar. The mass balance equation for oxygen in the liquid is expressed as follows:

$$\frac{dC}{dt} = k_L a(C^* - C) \tag{3}$$

Where C and C^* are the concentration (g l^{-1}) and the solubility (g l^{-1}) of O_2 in the liquid, respectively, and t the time (s). Considering the homogeneous liquid phase and using as boundary condition, C_0 the O_2 concentration at $t = 0$, the integration of Equation 3 led to Equation 4 in which $k_L a$ is determined by plotting $Ln(C^* - C)$ over the time (t):

$$Ln(C^* - C) = Ln(C^* - C_0) - k_L at \tag{4}$$

For both equations 3 and 4, the $k_L a$ is referred to the liquid volume and not to the dispersion volume. According to Equation 4, the $k_L a$ is determined by the slope of the linear zone using the statistical *Test F* method developed by Ferreira et al. (2015), Mena et al. (2011). This method establishes the optimum number of points (n_p) for a linear regression of the experimental data, avoiding possible errors associated with the choice of the linear zone. The response time of the oxygen electrode (less than 0.8 s) was much smaller than the time required for mass transfer (6 to 260 s).

2.3. Bubble size distribution and mean bubble size

To obtain the bubble size distribution (BSD) and, consequently, the specific interfacial area (a) several sets of images (1024x768 pixels) for all operational conditions defined in Table 1 (the same conditions of the $k_L a$ determinations) were acquired using a colour digital video camera (Leica, DMS 300) (frame rate of 60 images s^{-1}) placed at the mid-height of the reactor and connected to a PC. To minimize the optical distortion of the collected images due to the reactor wall curvature, a Perspex rectangular box filled with water was fitted at half away height of the reactor. After the acquisition, the recorded images were identified and classified according to the image analysis technique using the software MATLAB R2020b (Ferreira et al., 2012). The image analysis involved the following procedure (presented in Fig. 2): (i) threshold (reduction of the colour depth of the image to 2 colours); (ii) hole fill (holes inside objects are filled); (iii) border kill (objects touching the board of the image are eliminated); (iv) noise elimination (applying a sequence of erosions to eliminate undesirable objects and a reconstruction to recover the original shape of the objects); (v) labelling the image (the objects are detected and identified).

[Figure 2 here]

For each image several numerical descriptors were calculated, being the equivalent diameter (D_{eq}) the only one presented here (Equation 5). Based on the observations, the bubbles were close to spherical geometry, thus, the size of each bubble was determined using the projected area of each bubble given by the image analysis methodology, according to Equation 5:

$$\mathrm{D_{eqi}} = \sqrt{\frac{4\mathrm{A_{proji}}}{\pi}} \tag{5}$$

Where $\mathrm{A_{proji}}$ is the bubble projected area. The BSD is usually represented by the Sauter mean diameter, (d_{32}, i.e., the diameter of a sphere with the same volume-to-surface ratio as the gas bubble) (Gonçalves et al., 2021) which is obtained by Equation 6:

$$\mathrm{d_{32}} = \frac{\sum_i \mathrm{n_i D_{eqi}^3}}{\sum_i \mathrm{n_i D_{eqi}^2}} \tag{6}$$

Where D_{eqi} represents the equivalent diameter of a bubble (m) and n_i the number of bubbles having the considered diameter. For each combination of the operating conditions (presented in Table 1), about 100 bubbles were analysed, in order to obtain the BSD with a statistical meaning (Ferreira et al., 2012) and a deviation smaller than 10% for d_{32} determination.

2.4. Gas holdup and specific interfacial area

The gas holdup (ε_G) was obtained by measuring the liquid height in the presence (h) and absence of gas (h_0) using a high-speed digital camera for greater accuracy. The ε_G was determined by Equation 7:

$$\mathrm{\varepsilon_G} = \frac{\mathrm{h - h_0}}{\mathrm{h}} \tag{7}$$

Based on ε_G and BSD measurements, the specific interfacial area, a, was obtained as follows:

$$a = 6\frac{\varepsilon_G}{d_{32}} \tag{8}$$

2.5. Bubble chord length

It is important to highlight that at high oscillatory conditions ($x_0 = 19$ mm, $f = 3$ to 4 Hz), in ethanol aqueous solutions, it was impossible to distinguish the bubbles on images due to the foam's formation. In these conditions, to have an approximate measurement of the bubble size over photography analysis, the mono-fibre probe was considered. The bubble chord length was then measured using an optical mono fibre probe (conical probe, type 1C Probe", A2 Photonic Sensors Ltd., Grenoble, France) as previously adopted by Mena et al. (2008) in a three phase BC and Ferreira et al. (2015) in an OFR-SPC. As the fibre tip pierces the bubble, the software So2_4 detects a signal, which is represented in Fig. 3. The V_G, V_L and V_B values were around 3.4, 0.5 and 0.16 volt respectively, for ethanol and sucrose solutions.

[Figure 3 here]

The bubble rise velocity was measured through the rising time (T_M) of the signal. This rising time was itself measured between two points defined as a percentage of the total amplitude. For these conical probes, the selection criteria for the thresholds were the following ones: (i) the thresholds need to frame the quasi-linear portion of the rising edge of the signal (avoiding the rounded portions at the start and end of the rising edge); (ii) the lowest (10 %) and the highest (90 %) thresholds must be adopted. The bubble rise velocity is determined using a correlation between T_M and the bubble velocity (Mena et al., 2008). This correlation by the probe calibration is performed according to the expression:

$$v_b = AT_m^B \tag{9}$$

Where A is 47.13, B is -1 and v_b the bubble rise velocity (m s^{-1}). The bubble chord length is calculated from the bubble rise velocity (v_b) and the residence time, as follows:

$$d_c = v_b \times T_G \tag{10}$$

Where T_G represents the time spent within a bubble (s) and d_c the bubble chord length (m). Given the impossibility of visualizing bubbles in the aqueous ethanol solution (formation of foam), under high oscillatory conditions ($x_0 = 19$ mm, $f = 3$ and 4 Hz), it was assumed that the d_c was d_{32}, because the bubbles are very small, and the estimated errors are meaningless at those conditions.

2.6. Power density

The power consumption inherent to the OFR-SPC operation was determined through the power density (P/V), a parameter that quantifies the power consumed per unit of volume. The power density was estimated applying the quasi-steady flow model according to Equation 11:

$$\left(\frac{P}{V}\right)_o = \frac{2\rho N_b}{3\pi C_D^2}\frac{1-\alpha^2}{\alpha^2}x_0^3\omega^3 \tag{11}$$

Where ρ represents the liquid density (kg m^{-3}), N_b the number of baffles per unit length (m^{-1}), C_D the orifice discharge coefficient (taken as 0.7), α the baffle cross-sectional area defined as $(d_0/D)^2$, x_0 the oscillation amplitude (m), ω oscillation angular frequency defined as $2\pi f$ (Hz).

Also, the specific power dissipation due to the rising bubbles was determined as follows:

$$\left(\frac{P}{V}\right)_B = \rho g u_g \tag{12}$$

Where g is the gravitational constant (m s^{-2}) and u_g the superficial gas velocity (m s^{-1}). The overall power density is given by the following expression:

$$\left(\frac{P}{V}\right) = \left(\frac{P}{V}\right)_o + \left(\frac{P}{V}\right)_B \tag{13}$$

2.7. Statistical analysis

2.7.1. Design of Experiments methodology

The Minitab 19 software was used to perform the Design of Experiments (DoE) approach. The DoE is a statistical methodology implemented in this study to investigate the effect and the relationship between each one of the following 4 factors, u_g, f, x_0, viscosity or surface tension with the response variable, $k_L a$. For that, it was carried out a 2^n factorial approach in which n represents the number of factors to be used ($n = 4$ factors), and each factor is represented with two levels, the lowest and the highest, as detailed in the matrix design, **Error! Reference source not found.** and **Error! Reference source not found.** from supplementary material, for sucrose (u_g, f, x_0 and viscosity effects) and ethanol (u_g, f, x_0 and surface tension), respectively. Control experiments using distilled water were performed for the $k_L a$. The factorial design was augmented by including a central point to evaluate the response curvature of each factor. The central point corresponds to the middle of each factor and axial points to the centred face as shown in Fig. 4 (Montgomery, 2000).

[Figure 4 here]

To analyse the effect of the liquid properties - surface tension and viscosity - on gas-liquid mass transfer, a comparison between water and Ethanol solution and water and sucrose solution (Table 2), respectively, was performed.

2.7.2. Analysis of variance

Analysis of variance (ANOVA) was used to study the influence of the operational conditions (x_0, f, u_g) and liquid properties (surface tension and viscosity) on the response variables k_L, a and d_{32}. Only these response variables were analysed since the others response variables, ε_G and $k_L a$ are obtained from them. These analyses were also performed using a statistical Minitab 19 software, considering a significance level p of 0.05.

3. Results and Discussion

Operating conditions, involving oscillatory conditions (i.e., oscillation amplitude and frequency) and superficial gas velocity are crucial parameters in controlling the hydrodynamics (i.e., gas holdup, bubble size distribution, flow regime, liquid velocity and bubble rise velocity) and mass transfer characteristics in the OFR-SPC. Like operating conditions, the variation of the liquid phase properties, comprising surface tension and viscosity must be taken into account when analysing the OFR performance. Likewise, it is essential to know the influence of liquid properties under different operating conditions.

3.1. Effect of operating conditions on the volumetric liquid-side mass transfer coefficient

Fig. 5 presents the experimental volumetric liquid-side mass transfer coefficient ($k_L a$) results obtained in the OFR-SPC operating under different operational conditions, i.e., oscillation amplitude

ranging between 4×10^{-3} and 1.9×10^{-2} m, oscillation frequency ranging between 1 and 4 Hz and superficial gas velocity (u_g) ranging from 2×10^{-3} to 9.8×10^{-3} m s^{-1} in the presence of ethanol (6.31% (w/v)), Fig. 5A, and sucrose (48.3% (w/v)), Fig. 5B. The experiments were performed at superficial gas velocity ranging from 4.9×10^{-4} to 9.8×10^{-3} m s^{-1}. The results were only plotted for higher values of superficial gas velocity ranging from 2×10^{-3} to 9.8×10^{-3} m s^{-1}, since at lower superficial gas velocities, $< 2 \times 10^{-3}$ m s^{-1}, the $k_L a$ values varied between 0.005 and 0.015 s^{-1}, and consequently, the graph would not represent a big difference in colours with that operating conditions. The error estimated for $k_L a$ was on average less than 6 % using a 95 % confidence interval.

[Figure 5 here]

According to these data, both oscillatory conditions and superficial gas velocity showed a significant impact on $k_L a$ in the presence of ethanol and sucrose. Regarding the effect of oscillatory conditions, the analysis of Fig. 5 demonstrates that increasing the oscillation amplitude from 4 to 19 mm increased $k_L a$ values an average of 3-fold, for the two solutions used. Similarly, an increase in the oscillation frequency from 1 to 4 Hz also resulted in superior $k_L a$ values, an average of 2.5-fold. The mass transfer enhancement under these conditions can be explained by the intensification of the oscillatory motion which originates the formation and dissipation of eddies inside each SPC, reducing bubble size and enhancing bubble residence time, which in turn increases the gas holdup and the gas-liquid contacting area, and, hence, the $k_L a$. It should be noted that the presence of sucrose (Fig. 5B), when operating at high oscillation amplitude ($St = 0.062$), the increase in the oscillation frequency from 1 to 4 Hz resulted in a sudden increase in $k_L a$, since the oscillation amplitude typically allows the eddies to move along the OFR-SPC and the oscillation frequency promotes a radial effect on mixing, increasing bubble residence time, enhancing $k_L a$. Similar achievements regarding the effect of oscillations on $k_L a$ can be found in previous research works using OFR-SPC (Almeida et al., 2022; A Ferreira et al., 2015; Ferreira et al., 2017; Gonçalves et al., 2021; Reis et al., 2007), oscillatory baffled reactor (Ahmed et al., 2019, 2018; Oliveira and Ni, 2004; Pereira et al., 2014) and oscillatory constricted tubular reactor (Reis et al., 2008). However, in ethanol solutions (Fig. 5A), operating at constant oscillation amplitude of 19 mm and at constant u_g of 9.8 mm s^{-1}, higher values of oscillation frequency ($f = 3$ and 4 Hz) led to a slight decrease in $k_L a$ values from 0.120 ± 0.0005 to 0.106 ± 0.0001 s^{-1}, respectively. This decrease may be a result of the high oscillations, which promoted the formation of foam, hereby creating resistance to mass transfer, decreasing $k_L a$, or because the O_2 sensor probably measured in the foam and not in the ethanol solution, as it can be seen in **Error! Reference source not found.** and videos in supplementary material.

Regarding the effect of superfical gas velocity on $k_L a$, the analysis of Fig. 5 shows that increasing this parameter from 4.9×10^{-4} to 9.8×10^{-3} m s^{-1}, the $k_L a$ values increased an average of 5-fold for ethanol solutions (Fig. 5A) and about 7-fold for sucrose solutions (Fig. 5B). The improvement of $k_L a$ at higher u_g is a consequence of the greater quantity of the gas injected per unit of time. These results on

the effect of u_g on k_La are consistent with the observed in previous studies (Gonçalves et al., 2021). The significant effect of the tested operating conditions on k_La in the presence of ethanol and sucrose was confirmed by DoE methodology, as demonstrated in Pareto graph (**Error! Reference source not found.** and **Error! Reference source not found.** from the supplementary material for ethanol and sucrose respectively), where the u_g evidenced the highest effect, followed by f and x_0.

In addition, to analyse the effect of the liquid phase properties, surface tension and viscosity on k_La the DoE methodology was applied, and the Pareto graph was obtained. The absolute values of the standardized effects from the highest to the lowest are presented in Pareto graph (**Error! Reference source not found.** and **Error! Reference source not found.**), where the red reference line indicates which effects are statistically significant. The results indicate that the surface tension had no significant effect on k_La and the viscosity significantly decreased k_La. Regarding the interaction terms, they indicate a statistically significant effect in the systems studied: superficial gas velocity-amplitude; superficial gas velocity-frequency; frequency-amplitude; superficial gas velocity-amplitude-frequency. The DoE approach, for the effects of surface tension and viscosity, generated the Equations 14 and 15, respectively, using central, axial and cube points:

$$\begin{aligned} \mathrm{k_La} \times 10^3 = {} & 36 - 0.53\sigma - 2118\mathrm{u_g} - 2.7\mathrm{x_0} - 4.6\mathrm{f} + 61\mathrm{u_g}\sigma + 0.048\sigma\mathrm{x_0} \\ & + 0.088\sigma\mathrm{f} + 1314\mathrm{u_g x_0} + 4837\mathrm{u_g f} + 0.95\mathrm{x_0 f} - 20.9\sigma\mathrm{u_g x_0} \\ & - 71\sigma\mathrm{u_g f} - 0.015\sigma\mathrm{x_0 f} - 647\mathrm{u_g x_0 f} + 12.42\sigma\mathrm{u_g x_0 f} \end{aligned} \quad (14)$$

$$\begin{aligned} \mathrm{k_La} \times 10^3 = {} & -2.7 + 1.38\mu + 2286\mathrm{u_g} + 1.28\mathrm{f} + 1.12\mathrm{x_0} - 232\mu\mathrm{u_g} - 0.45\mu\mathrm{f} \\ & - 0.368\mu\mathrm{x_0} - 385\mathrm{u_g f} - 215\mathrm{u_g x_0} - 0.27\mathrm{f x_0} + 11\mu\mathrm{u_g f} + 6.6\mu\mathrm{u_g x_0} \\ & + 0.127\mu\mathrm{f x_0} + 276.8\mathrm{u_g f x_0} - 17\mu\mathrm{u_g f x_0} \end{aligned} \quad (15)$$

Where σ (mN m^{-1}) represents the surface tension of ethanol solution, μ the viscosity of sucrose solution (cP), u_g the superficial gas velocity (m s^{-1}), f the frequency (Hz) and x_0 the amplitude (mm).

It is noteworthy that the experimental k_La results showed a good agreement (with a relative error less than 20-40 %) with the k_La results obtained from DoE equations, as Fig. 6 illustrates, which means that equations 14 and 15 from DoE modulated very well, for all the operating conditions tested.

[Figure 6 here]

3.2. Effect of operating conditions on gas holdup

The measurements of the gas holdup (ε_G) given by the operational conditions, for the ethanol (6.31 % (w/v)) and sucrose (48.3 % (w/v)) solutions are presented in Fig. 7 as a function of the superficial gas velocity (u_g). The homogeneous and heterogeneous flow regimes presented in Fig. 7 were obtained visually through the photos taken with a high-speed digital video camera.

[Figure 7 here]

From graphs of Fig. 7 it is possible to observe that ε_G is clearly influenced by the operational conditions, having the superficial gas velocity the highest impact. Increasing this parameter from 0.5 to

9.8 mm s^{-1} strongly increased ε_G values, an average of 15-fold. The improvement of ε_G at higher u_g is the result of the greater amount of gas injected per unit of time, increasing a and ε_G (Almeida et al., 2022; Gonçalves et al., 2021). Regarding the effect of the oscillatory conditions, the analysis of Fig. 7B and Fig. 7C demonstrates that higher oscillations ($x_0 > 9$ mm, $f > 2$ Hz) influenced the flow regime (a homogeneous regime is predominant) and consequently increased ε_G values from 1.3 to 2-fold. The increase in ε_G in response to high oscillations was a consequence of the increment in the residence time of the bubbles that become trapped, as a result of the formation of vortices promoted by intense oscillations. Instead, lower oscillation amplitudes (x_0 < 9 mm) and frequencies ranged from 1 to 4 Hz reduced ε_G values, about 1.5-fold (Fig. 7A). This decrease in ε_G may be associated with the low intensity of the eddies' propagation and its rapid destruction, as frequency increases from 1 to 4 Hz. Consequently, bubbles coalesced and did not become trapped inside the vortices and bubble rise velocity ($2\pi f x_0$) increased, as it can be seen in the two videos from the supplementary material, for ethanol, recorded at $x_0 = 4$ mm, $u_g = 9.8$ mm s^{-1} and $f = 1$ and 4 Hz, respectively. Therefore, oscillatory conditions had remarkable effect on ε_G, it decreased at low oscillations and increased at higher, justified by a combined effect of a decrease in d_{32} and an increase in bubble residence time. Similar results on the effect of oscillatory conditions on the ε_G have already been reported in the literature. For example, Gonçalves et al. (2021) in an OFR-SPC demonstrated a dual behaviour for the ε_G, it decreased at low oscillation amplitudes (between 4 and 9 mm) and frequencies (1-1.5 Hz), being practically constant for oscillation amplitudes and frequencies higher than 9 mm and 1.5 Hz, respectively. Likewise, Almeida et al. (2022) in an OFR-SPC encountered two behaviours for ε_G, it decreased about 1.4-fold at low oscillation amplitude of 4 mm and frequencies ranging from 1 to 4 Hz and it increased at higher oscillation amplitude of 19 mm an average of 1.6-fold. Also, Oliveira and Ni (2004) in an oscillatory baffled reactor observed a dual effect for the ε_G, in which low oscillations barely affected the ε_G, whereas higher oscillatory conditions ($f > 4$ Hz) significantly improved the ε_G. Similar conclusion was revealed by Reis et al. (2008) operating an oscillatory constricted-tubular reactor, ε_G decreased at constant oscillation amplitude ($x_0 = 1$ mm) and lower frequencies ($f < 10$ Hz), whereas higher oscillation frequencies ($f > 10$ Hz) enhanced ε_G. The significant influence of oscillations on ε_G was also confirmed through ANOVA analysis ($p < 0.05$).

The dual behaviour of the ε_G and the bubbles' dynamics promoted by the low and high oscillations of the liquid and by the superficial gas velocity explain the different flow regimes encountered in the OFR-SPC in this study: (i) at low oscillations ($x_0 < 9$ mm, $f = 1$ and 2 Hz), for $D = 16$ mm, a slug flow was identified with the presence of spherical-cap bubbles (as it can be seen on graphical abstract); (ii) at oscillation amplitude of 9 mm, frequency of 2 Hz and $u_g > 6$ mm s^{-1} a transition operating regime was identified; (iii) by further increasing oscillations ($x_0 > 9$ mm, $f = 3$ and 4 Hz), a homogeneous regime (bubbly flow) was predominant for all range of superficial gas velocity tested, where high ε_G values were accompanied by small bubbles' size, providing an increased gas-liquid interfacial area. These operating

conditions as those identified for flow regimes are of the same order of magnitude of those found by Ahmed et al. (2018), even for a low *D* of 10 mm, in pure systems using an OFR-SPC.

3.3. Effect of operating conditions on the Sauter mean bubble diameter

In Fig. 8 is exhibited an example of bubble size distribution (BSD) curve obtained through the image analysis technique, under constant oscillation amplitude of 4 mm, frequencies of 1 and 4 Hz and constant superficial gas velocity of 1.0 mm s^{-1}, operating with ethanol (6.31% (w/v)) and sucrose (48.3 % (w/v)) aqueous solutions.

[Figure 8 here]

Fig. 8 shows that the BSD curve is in general bimodal either for the ethanol or for sucrose solutions. The peak with low bubbles percentage has high D_{eq} values, which might be related to the bubbles passing through the SPC, where the inner diameter (d_0) is smaller, and even because the oscillations are still low ($x_0 = 4$ mm) enough to break the bubbles, causing the bubbles coalescence. In contrast, increasing oscillation amplitude from 4 to 19 mm and oscillation frequency from 1 to 4 Hz, that peak tended to disappear, which means that bubble's size decreased with the increase in oscillations, resulting, in most cases, in a modal distribution with one peak at low D_{eq} values. According to Fig. 8, in ethanol solutions, an increase in the oscillation frequency from 1 to 4 Hz, in which the peak with the highest intensity has shifted a bit to the right (with a longer tail), resulted in a slight increase of bubbles' size, and consequently, in d_{32} values from 0.086 ± 0.021 to 1.11 ± 0.045 mm, which was not expected. This increase in bubble's size may be related to the low oscillation amplitude ($x_0 = 4$ mm) where the area occupied by the eddies is still low enough to break tiny bubbles created by the ethanol in which bubbles' size is lower ($d_{32} = 0.086 \pm 0.021$). So, an increase in the oscillatory movement (in this case by increasing frequency from 1 to 4 Hz) may occasionally promote the displacement of bubbles into coalescence phenomenon, i.e., the reciprocating movement of the liquid retards the upward movement of the rising bubbles, resulting in the formation of large bubbles. However, according to Reis et al. (2007) the formation of large bubbles in pure systems requires a faster reciprocating movement, i.e., higher oscillation frequencies ($f = 20$ Hz), since water does not inhibit bubbles' coalescence. The influence of ethanol on BSD and on bubbles' shape was also studied by Besagni and Inzoli (2019) in a BC who noticed that the presence of ethanol moved the BSD slightly towards low D_{eq} values, with multiple relative maxima. Likewise, high viscous medium is known for promoting bubble coalescence by decreasing bubble rate with a bimodal BSD. Mouza et al. (2005) observed a bimodal BSD in a BC at higher viscosity ($\mu = 8.2$ cP – Glycerine), due to drag forces, which promote coalescence in the sparger region. Yang et al. (2010) operating a BC also found two peaks, $0.7 < d_{eq} < 10$ mm and $d_{eq} > 10$ mm, just like Philip et al. (1990) reported two peaks, $d_{eq} < 1$ mm and $d_{eq} > 20$ mm. Unlike common contactors, in the OFR-SPC the intensity of the second peak could be attenuated by improving the oscillatory conditions on the liquid originating a modal BSD, as explained above. In the present work, despite of the bimodal distribution with a second low intensity peak, it was quite reasonable to use the normal distribution to estimate the 95 % confidence intervals associated with d_{32}.

Fig. 9 presents the evolution of the Sauter mean bubble diameter (d_{32}) determinations in response to several operational conditions, operating with ethanol (6.31 % (w/v)) and sucrose aqueous solutions (48.3 % (w/v)), Fig. 9A, and Fig. 9B, respectively.

[Figure 9 here]

Fig. 9 indicates that increasing oscillation amplitude from 4 to 19 mm and frequency from 1 to 4 Hz, d_{32} values decreased on average of 2.5-fold, for both ethanol and sucrose solutions. The decrease observed in d_{32} at higher oscillatory conditions ($x_0 > 9$ mm, $f > 3$ Hz) is a consequence of the periodic formation and dissipation of eddies in radial and axial directions, which break the bubbles into smaller and more uniform sizes, spreading uniformly, and covering the whole area in the SPC. Under lower oscillatory conditions ($x_0 < 9$ mm, $f < 3$ Hz), the bubbles' coalescence owing to the SPC of the OFR might have occurred, keeping d_{32} practically constant for $u_g > 4$ mm s^{-1}, either in the presence of ethanol or sucrose. The error estimated for d_{32} was a bit higher (< 16 %), as result of the low oscillations, which are not enough to create uniform bubbles. According to Oliveira and Ni (2004), at low oscillations, the bubble size may be influenced by the superficial gas velocity and the type of the sparger. Similar accomplishments concerning the effect of oscillations on d_{32} behaviour can be found in previous research works using OFR-SPC (Almeida et al., 2022; A Ferreira et al., 2015; Ferreira et al., 2017; Gonçalves et al., 2021; Reis et al., 2007), oscillatory baffled reactor (Ahmed et al., 2019, 2018; Oliveira and Ni, 2004; Pereira et al., 2014) and oscillatory constricted tubular reactor (Reis et al., 2008). For evaluating the effect of oscillations on d_{32}, **Error! Reference source not found.** in supplementary material is presented. For the ethanol the effect of oscillations on d_{32} was not so evident as for sucrose. Whereas for ethanol, at constant amplitude of 4 mm and frequencies 1 and 4 Hz the d_{32} decreases from 3.33 ± 0.55 to 1.51 ± 0.05 mm (**Error! Reference source not found.**A), instead for the sucrose, at the same oscillatory conditions the d_{32} decreases from 6.25 ± 0.61 to 1.86 ± 0.12 mm (**Error! Reference source not found.**B), which was more notorious. The reason for the smaller decrease for the ethanol (~2-fold decreasing) is that ethanol is responsible for bubble coalescence inhibition causing the appearance of bubbles with smaller sizes. These smaller bubbles have low surface area ($4\pi r^2$) and when oscillations are imposed on the liquid the contact area between bubbles and the eddies (caused by oscillations) is lower making it almost impossible to break smaller bubbles.

Regarding the effect of u_g on d_{32}, the data in Fig. 9 evidence that at lower oscillation amplitudes ($x_0 < 9$ mm) the increase in the superficial gas velocity (up to 9.8 mm s^{-1}) increased the d_{32}, an average of 1.5-fold for ethanol solutions (Fig. 9A) and 3.5-fold for sucrose (Fig. 9B) by promoting the bubbles' coalescence. It should be noted that the d_{32} increase in ethanol solutions was less significative because it inhibited bubble's coalescence. Regarding the experimental results performed at higher oscillatory conditions ($x_0 > 9$ mm, $f > 3$ Hz), the bubbles became with uniform size (error less than < 7 %, for d_{32}) and very tiny, with a rigid behaviour, and almost impossible to break (Fig. 9). Therefore, in these oscillation conditions the superficial gas velocity had no significant effect on d_{32}, a remark also observed in the studies performed by Ni and Oliveira (2004), Reis et al. (2008, 2007), Ferreira et al. (2015) in pure

(distilled water) systems and Gonçalves et al. (2021) in microalgal cultures. According to the ANOVA analysis (**Error! Reference source not found.** and **Error! Reference source not found.** from supplementary material), the oscillation frequency evidenced a considerable influence on d_{32} ($p < 0.05$) for both ethanol and sucrose aqueous solutions, instead, oscillation amplitude only had major influence on d_{32} ($p < 0.05$) in sucrose solutions. The effect of amplitude on d_{32} ($p > 0.05$) is attenuated in ethanol aqueous solutions because ethanol inhibits bubble's coalescence.

An important aspect to highlight from the analysis of Fig. 9A is the fact that at the highest oscillatory conditions studied ($x_0 = 19$ mm, $f = 4$ Hz) the presence of ethanol led to the formation of foam (which was not expected). Therefore, in these conditions it was not possible to visualize the bubbles through the high-speed digital video camera, so the optical fibre technique was preferred to measure the bubble chord length over the image analysis technique. Besagni et al. (2016) proposed a method to convert the bubble chord distribution into BSD. This method is based in two assumptions: (i) two-dimensional plane; (ii) bubbles rising vertically. However, in the OFR-SPC this method is discarded due two reasons, on the one hand, in the OFR-SPC specifically at these oscillations ($x_0 = 19$ mm, $f = 4$ Hz) in the presence of ethanol the bubbles tend to be kept inside the eddies, so the bubbles do not rise vertically but rise by exploring all the trajectories of the eddies within the SPC. On the other hand, owing to the oscillations, it is not known the number of times the fibre pierces the same bubble, making the measurement of d_c probably less accurate. Considering these two reasons, it was still quite reasonable to assume d_c as being d_{32}, because the bubbles are very small, and the estimated errors are meaningless at those conditions.

3.4. Effect of operating conditions on the liquid-side mass transfer coefficient and specific interfacial area

The specific interfacial area (a) was calculated from ε_G and d_{32} values using Equation 8. With a determined, the liquid-side mass transfer coefficient, k_L was then obtained from experimental $k_L a$ values. The evolution of k_L and a values as a function of d_{32} determinations in response to different oscillatory conditions are presented in Fig. 10, for ethanol (Fig. 10A) and sucrose aqueous solutions (Fig. 10B). Fig. 10 shows a comparison between the experimental k_L results and the ones obtained in previous research work (Almeida et al., 2022) which are represented through lines (not fitted lines). This comparison was only made for the k_L since the a results were similar.

[Figure 10 here]

Regarding the k_L results presented in Fig. 10 demonstrate that oscillatory conditions significantly affect the k_L in the presence of ethanol or sucrose. Typically, high oscillations tend to promote convective phenomena around bubbles, decreasing the film-thickness around them, enhancing k_L. Moreover, considering the decrease observed in d_{32} for higher oscillatory conditions, an increase in k_L was expected, as it was proven in a previous research paper by Almeida et al. (2022), when studying the

influence of electrolytes on gas-liquid mass transfer (Fig. 10A). However, in the present study a different behaviour was observed for k_L in ethanol aqueous solutions as demonstrated in Fig. 10A. According to these data, at high oscillatory conditions, the k_L tends to decrease as d_{32} decreases, probably consequence of the disposal of the small bubbles close to each other promoted by the high oscillation amplitude ($x_0 = 19$ mm) i.e., low St numbers (0.062). This disposal of the bubbles affects the diffusion way of the gas into the liquid surrounding the bubbles, leading to low k_L values - bubble swarms, shown in the figure of graphical abstract for ethanol and compared with water in Fig. 11. Besides that, either the bubble's contamination from ethanol or the formation of foam, already mentioned, could explain the k_L decrease obtained in this study, face to pure (distilled water) systems (Fig. 11). A decrease in k_L was also reported by Baz-Rodríguez et al. (2014), using a BC, attributed to the reduction of slip velocity between gas and liquid phase caused by the bubbles swarm, which tends to appear as gas holdup increases due to the high bubble's residence time.

Unlike ethanol solutions (Fig. 10A), in sucrose aqueous solutions, the k_L increased as d_{32} decreased as the analysis of Fig. 10B demonstrates. This kind of behaviour was similar when studying the influence of electrolytes on gas-liquid mass transfer (Almeida et al., 2022). In fact, higher oscillatory conditions ($x_0 = 19$ mm, $f = 2$ to 4 Hz) resulted in superior k_L values. However, these oscillation conditions have not contributed to significant changes in d_{32}, which remained approximately constant (Fig. 9), but it might have contributed to high oscillatory velocity over the liquid, causing predominance of the convective phenomena, which leads to an increase in the renewal rate of the liquid film at the interface, increasing k_L. Hence, the increase observed in $k_L a$, (as described in section 3.1) under these oscillatory conditions was mostly due to an increase in k_L rather than an increase in a, since a is dependent on d_{32} and this remained constant. By applying ANOVA analysis (**Error! Reference source not found.** and **Error! Reference source not found.**) it was proven that, in general, oscillation amplitude had a significant effect on k_L ($p < 0.05$) for both ethanol and sucrose solutions, while oscillation frequency only had a significant effect ($p < 0.05$) for the ethanol solutions.

Regarding the a results, the analysis of Fig. 10 clearly shows that a increases as oscillatory conditions increase, either for ethanol or sucrose solutions. At constant oscillation amplitude of 4 mm, increasing frequency from 1 to 4 Hz the a value increased an average of 2.5-fold, probably due to the d_{32} decrease. At the highest oscillation amplitude studied ($x_0 = 19$ mm), an increase in oscillation frequency from 1 to 4 Hz resulted in a superior a increase, an average of 3.5-fold, which may be related to an increase in ε_G (bubbles become stuck inside the eddies, as already mentioned). These results suggest that at the lowest oscillation amplitude studied ($x_0 = 4$ mm) the a is more influenced by d_{32}, whereas, at the highest oscillation amplitude studied ($x_0 = 19$ mm) is affected by ε_G. According to the results from ANOVA analysis (**Error! Reference source not found.** and **Error! Reference source not found.**) both the oscillatory conditions evaluated, and the presence of sucrose had a significant effect on a ($p < 0.05$) instead, for ethanol solutions, oscillation amplitude revealed a negligible influence on a ($p > 0.05$).

Ethanol sufficiently inhibits bubbles coalescence, which explains the discrepancy observed on a between the two solutions tested.

3.5. Effect of liquid surface tension and viscosity on gas-liquid mass transfer

In order to analyse the influence of liquid properties on the different parameters studied (ε_G, d_{32}, k_La k_L and a) the Fig. 11 was represented through the average experimental values of the ε_G, and d_{32} (Fig. 11A), and of the k_La, k_L and a (Fig. 11B), for all operational conditions, as function of ethanol and sucrose aqueous solutions along with 95 % confidence interval. These values are also compared with the ones obtained in distilled water by Ferreira et al. (2015) in an OFR-SPC.

[Figure 11 here]

The experimental ε_G results shown in the Fig. 11A indicate that the presence of ethanol and sucrose had no significant influence on ε_G, within the range of operational conditions evaluated in this study, for the two solutions tested (proved by ANOVA analysis, $p > 0.05$). The ε_G behaved similarly in the presence of ethanol and sucrose. These observations are not in agreement with the widely reported in the literature, in which ε_G increases with the decrease of the surface tension and viscosity and tends to decline with the increment of viscosity. For example, Mouza et al. (2005) in a BC concluded that lowering the surface tension (up to 48 mN m^{-1}) of butanol slightly increased ε_G. Freitas and Teixeira (1998) evaluated the effect of the surface tension on the hydrodynamics using a three phase airlift reactor and demonstrated that the presence of ethanol (10 g/l) increased ε_G. Zahradník et al. (1997) in their studies on flow regime and using a BC revealed that the increase of alcohol chain length, in aliphatic alcohols, resulted in an increase in the ε_G. In a study performed by El Azher et al. (2005) the authors compared three different alcohols (ethanol, propanol and butanol), using an airlift reactor and found that butanol presented the highest gas holdup. The authors also claimed that ethanol promotes bubble coalescence inhibition leading to a bubble recirculation in downcomer, which in turn explains the increase observed in gas holdup.

In what concerns to the effect of viscosity on ε_G, there is a dual effect in previous investigations, it increased at lower liquid viscosity, and it decreased with the increment of viscosity (Yang et al., 2022). For example, Besagni et.al., (2017) who investigated in detail the effect of liquid viscosity on the ε_G in a BC stated that the viscosity has a dual effect on ε_G: (i) at low viscosity, the bubble coalescence is limited, and the large drag force reduces the bubble rise velocity causing an increase in the ε_G; (ii) on the contrary, at high viscosity the bubbles tend to coalesce, resulting in the formation of large bubbles rising through the BC with higher velocity, thus reducing the ε_G. The decrease in ε_G was also identified by Zahradnik et al., (1997) at moderate/high viscosities of saccharose ($3 < \mu < 100$ cP) using a BC. The dual effect of viscosity on ε_G was also perceived by Snape et al. (1992) in their study on hydrodynamics with sucrose solutions and using an external loop airlift reactor. This study demonstrated that low sucrose concentrations resulted in an increase in ε_G, in opposite, higher concentrations led to lower ε_G

values. At the highest sucrose concentrations (8 % (w/v)) the ε_G values were still lower than those obtained for water. These findings exemplify the difference between the experimental ε_G results registered in the OFR-SPC and those reported for BC and airlift reactors, either in the presence of ethanol or sucrose. This discrepancy might be due to the oscillations imposed on the liquid, which promote the renewal of the bubble's surface, hereby increasing bubble rise velocity/or due to the vortices formed that maintain the bubbles kept inside. In our previous research work, the present authors supported the two explanations for the negligible effect of electrolytes concentration on ε_G: (i) the non-occurrence of bubble coalescence inhibition over a wide range of electrolytes concentrations; (ii) the chemical structure of the compound (Almeida et al., 2022).

It is known that the addition of an alcohol to an aqueous solution can reduce the surface tension, resulting in a small mean bubble diameter and in an increased interfacial area. Comparing the d_{32} data from pure (distilled water) and non-pure (ethanol and sucrose) systems presented in Fig. 11, it is evident that in the presence of ethanol, surface tension decreased, and consequently d_{32} values decreased (~2-fold), from 2.52 mm to 1.42 ± 0.07 mm, and, hence, the specific interfacial area was notably increased from 70 m^{-1} to 129 ± 4 m^{-1}, a remark also demonstrated by Mouza et al. (2005) and Maceiras et al. (2010) in BCs. A decrease in liquid surface tension (ethanol) favours the formation of small bubbles by promoting bubbles' breakage and demoting coalescence, reducing d_{32}, hereby increasing the specific interfacial area, an explanation also given by Mouza et al. (2005) in their studies on the effect of liquid properties and by Besagni and Inzoli (2019) through BSD studies. The ANOVA statistical analysis demonstrated a significant influence of ethanol (surface tension) on d_{32}, and, hence on a values ($p < 0.05$).

In a recent research article published by the same authors regarding the influence of electrolyte concentrations (HCl, NaOH and NaCl) stated that below the c_t the SPC design was responsible for the transition between the smaller bubbles formed near the sparger into bubble coalescence under low oscillations ($x_0 < 9$ mm and $f < 2$ Hz) as bubbles pass through the SPC (Almeida et al., 2022). This phenomenon observed at below the c_t was different from the airlift reactor and BCs. However, contrary to our previous research work, in the present study, it would be expected that the smaller bubbles generated in the presence of ethanol, would coalesce as these bubbles ascended along the OFR-SPC. Nevertheless, the bubbles remained with smaller sizes. This phenomenon can be seen in **Error! Reference source not found.** and in videos presented on supplementary material, which was the opposite to the observed in our previous work (Almeida et al., 2022). The reason that supports this conclusion is that ethanol are amphiphilic molecules and when mixed with water occurs a strong hydrogen bonding and, on the other hand, the ethanol is mainly adsorbed at the gas-liquid interface causing repulsive forces between gas and liquid, being responsible for bubble coalescence inhibition. Thus, the chemical nature of the compound must be extremely relevant for analysing bubble coalescence inhibition.

Unlike the ethanol, the sucrose (viscosity) had no significant influence on d_{32} and on a values: 2.36 ± 0.16 mm and 69 ± 3.4 m^{-1} respectively, compared to those ($d_{32} = 2.52$ mm and $a = 70$ m^{-1}) obtained with distilled water by Ferreira et al. (2015), probably due to the viscosity ($\mu = 3.33$ cP) used in this study, which favoured bubbles' coalescence. The insignificant influence of viscosity on d_{32}, and, hence on a, verified in the present work, was confirmed through the statistical analysis ($p > 0.05$) (**Error! Reference source not found.** and **Error! Reference source not found.**). This result is consistent with the observations of Mouza et al., (2005) where the viscosity (glycerine) ($\mu = 8.2$ cP) favours the formation of large bubbles by decreasing turbulence, which promotes bubble coalescence and prevents breakage, increasing d_{32}. Besagni et al. (2017) in their studies on the effect of viscosity on hydrodynamics found a dual effect of viscosity on bubble's size: low viscosities favour the formation of small bubbles and moderate/high viscosities favour the formation of large bubbles. Nevertheless, it was not notorious the effect of viscosity on d_{32} because the oscillations imposed on the liquid cause changes in the flow hydrodynamics, and, hence on d_{32}.

Considering the experimental $k_L a$ results obtained in the presence of ethanol and sucrose it can be suggested that: (i) the decrease in the surface tension (ethanol addition) increased the $k_L a$ an average of 1.4-fold (Fig. 11), in respect to pure (distilled water) systems, attributable to the a increase, rather than k_L, consequence of d_{32} reduction by inhibiting bubble coalescence (this effect was not considered statistically significant); (ii) the increase in the liquid viscosity (sucrose addition) decreased the $k_L a$ ~1.5-fold (Fig. 11), face to pure (distilled water) systems, by increasing the film thickness around the bubble, (Llewellin et al., 2012) and by reducing the oxygen diffusion coefficient, according to Lewis and Whitman's film theory.

From Fig. 11B it is also possible to observe that the increase in the liquid viscosity decreased k_L values, about 1.8-fold. These values are lower than those observed in pure (distilled water) systems. The decrease in k_L with the increase in viscosity may result from the increase in the film thickness surrounding the bubble or from the decrease in oxygen diffusion coefficient, this way, affecting the mass transfer (Alves et al., 2005), or from the contamination of the bubble from sucrose. On the other hand, it is also evident (Fig. 11B) that the decrease in the liquid phase surface tension reduced the k_L 1.5-fold, in relation to pure (distilled water) systems. This decrease in k_L in the presence of ethanol was not considered significant ($p > 0.05$), in opposite to sucrose solutions ($p < 0.05$), according to ANOVA analysis (**Error! Reference source not found.** and **Error! Reference source not found.**).

3.6. Comparison of gas-liquid mass transfer in the OFR-SPC and common gas-liquid contactors

Table 3 presents a comparison between the $k_L a$, ε_G, d_{32}, k_L and a values obtained in the OFR-SPC used in this study and those reported in the literature for BC and airlift reactors.

[Table 3 here]

According to the data presented in Table 3, the $k_L a$ values reported for BC and airlift ranged from 9 to 113 h^{-1} in ethanol solutions and from 7 to 36 h^{-1} in sucrose solutions, which are considerably lower than the ones obtained in this study, also operating with ethanol and sucrose aqueous solutions, using an OFR-SPC even operating at low oscillation values ($x_0 = 4$ mm, $f = 1$ Hz). Moreover, increasing oscillation amplitude from 4 to 19 mm and operating at constant frequency of 2 Hz led to higher $k_L a$ values, a maximum of 384 ± 10 h^{-1} and 185 ± 4 h^{-1} for ethanol and sucrose solutions, respectively, which are significantly higher, on average up to 2 to 6-fold, than those reported for BCs and airlift reactors, as shown in Table 3. In addition, it is also noteworthy that the k_L results obtained in the OFR-SPC are about 1.2-fold and 1.5-fold higher, for ethanol and sucrose aqueous solutions, respectively, than those obtained in BC (2012), which was expected as oscillatory conditions typically increase k_L. This substantial increment on $k_L a$ and k_L is a consequence of the oscillatory flow mixing inside the reactor and the SPC design, which promotes eddies propagation in radial and axial direction, resulting in mixing efficiencies. These results are encouraging and indicate that the OFR-SPC, under adequate conditions, can reach good gas-liquid mass transfer rates, even better than BC and airlift reactors.

Contrary, several studies in the literature using BC or airlift have reported that ethanol decreases k_L and bubbles' size by inhibiting bubbles' coalescence, and increases ε_G, being that sufficient to increase a and to result in an increase in the $k_L a$ values (Ferreira et al., 2012; Mouza et al., 2005). Instead, in sucrose solutions, ε_G, and k_L tended to decrease, promoting bubbles' coalescence, and, hence, reducing $k_L a$ (Besagni et al., 2017; J.Zahradník et al., 1997; Onken and Weiland, 1980). In contrast, in the present study, the liquid properties, surface tension and viscosity, revealed a negligible influence on ε_G, while bubbles' size was only affected by surface tension being the viscosity effect negligible.

Regarding power density, the OFR-SPC can also be more favourable. The power density results demonstrate that the OFR-SPC used in this study can ensure efficient gas-liquid mass transfer rates (2 to 6-fold higher), even without a significant increase in power density (~ 105 W m^{-3}), in opposite to BCs (~ 90 W m^{-3}) or airlift reactors (20 - 60 W m^{-3}), making this novel OFR-SPC with potential to be used in bioprocessing industry, replacing BC and airlift bioreactors.

4. Conclusions

In this study the influence of the liquid phase properties, surface tension and viscosity on the hydrodynamics and gas-liquid mass transfer characteristics under different operating conditions was studied for the first time in an OFR-SPC. Ethanol and sucrose aqueous solutions covering a range of surface tension and viscosity values were used.

The results presented indicate that liquid surface tension and viscosity had considerable effects on $k_L a$. A decrease in the liquid surface tension improved $k_L a$ up to 1.4-fold, totally attributable to the a increase, rather than k_L. An increase in the liquid viscosity resulted in a $k_L a$ decrease, up to 1.5-fold, attributable to the k_L decrease. Conversely, in general, increasing the oscillatory conditions and the

superficial gas velocity improved $k_L a$ either in the presence of ethanol or sucrose, an effect confirmed by DoE methodology results.

According to the experimental results, liquid surface tension and viscosity had no significant influence on gas holdup. However, the literature has reported an increase in ε_G in ethanol aqueous solutions and a decrease at moderate/high viscosities, for common gas-liquid contactors. In contrast, oscillatory conditions strongly affected the ε_G, it decreased at low oscillations and increased at higher.

It was found that bubble's size relies on the liquid properties and operational conditions. As expected, the decrease in the liquid surface tension provided the formation of small bubbles by demoting coalescence and promoting bubbles' breakage, reducing d_{32}, whereas an increase in the liquid viscosity favoured the formation of large bubbles by decreasing turbulence, promoting bubble coalescence, and hindering breakage, increasing d_{32}. Therefore, the presence of ethanol delays the homogeneous-heterogeneous regime transition. Superficial gas velocity increased d_{32} and oscillatory conditions notably decreased d_{32}, an average of 2.5-fold, confirmed by the image analysis technique. Although the literature reports a bimodal BSD curve for BC in a viscous medium, in contrast, in the OFR-SPC the increase in oscillatory conditions originate a modal BSD for the two solutions evaluated.

Moreover, higher oscillations ($x_0 = 19$ mm, $f > 2$ Hz), in which d_{32} values are low, had a remarkable effect on the k_L (not expected), depending on the solution used: (i) in ethanol aqueous solutions, k_L values reduced as a consequence of the bubbles' swarm or the formation of foam; (ii) in sucrose aqueous solutions, k_L values increased, mostly due to the presence of the convective phenomenon around the bubbles.

It is concluded that oscillatory conditions govern the significant changes in the hydrodynamics and mass transfer in the OFR-SPC, via the reduction of bubble's size and the consequent increment in a and ε_G. The OFR-SPC exhibited notable $k_L a$ enhancement, up to 2-6-fold, compared to BC and airlift, even with moderate power consumption ($\sim$105 W m^{-3}). The $k_L a$ results presented in this study are rather encouraging and suggest that the OFR-SPC is a recommended technology to be used in gas-liquid bioprocesses, where the mass transfer and the liquid properties are important.

Acknowledgements

This work was financially supported by: I) Project PTDC/QEQ-PRS/3787/2014 -POCI-01-0145-FEDER-016816 - funded by the European Regional Development Fund (ERDF) through COMPETE2020 -Programa Operacional Competitividade e Internacionalização (POCI) and by national funds through Fundação para a Ciência e a Tecnologia.I.P. (FCT) - Project 9471 - Reforçar a Investigação,o Desenvolvimento Tecnológico e a Inovação; II) IF exploratory Project [IF/01087/2014] funded by FCT; III) LA/P/0045/2020 (ALiCE), UIDB/00511/2020 and UIDP/00511/2020 (LEPABE), funded by national funds through FCT/MCTES (PIDDAC); IV) the FCT under the scope of the strategic funding of UIDB/04469/2020 unit, and by LABBELS – Associate Laboratory in Biotechnology, Bioengineering and Microelectromechnaical Systems, LA/P/0029/2020. A. Ferreira is an Investigador FCT. F. Almeida would wish to thank to FCT for PhD scholarship 2020.05246.BD.

Notation

Abbreviations

BC	Bubble column
BSD	Bubble size distribution
DoE	Design of experiments
OFM	Oscillatory flow mixing
OFR	Oscillatory flow reactor
SPC	Smooth periodic constrictions

Symbols

V_B	Amplitude of the noise of the signal peak to peak, volt
d_c	Bubble chord length, m
A_{proji}	Bubble project area, m^2
v_b	Bubble rise velocity, m s^{-1}
L_1	Constriction length, m
c_t	Electrolyte transition concentration, mol l^{-1}
D_{eq}	Equivalent diameter, m
C_0	Gas concentration at initial time in liquid, g l^{-1}
C	Gas concentration in liquid, g l^{-1}
V_G	Gas level voltage, volt
C^*	Gas solubility, g l^{-1}
g	Gravitational constant, m s^{-2}
D	High threshold, dimensionless
D	Inner diameter of the straight section, m
d_0	Internal tube diameter in the constrictions, m
h_0	Liquid height in the absence of gas, m
h	Liquid height in the presence of gas, m
V_L	Liquid level voltage, volt
k_L	Liquid-side mass transfer coefficient, m s^{-1}
C	Low threshold, dimensionless
N_b	Number of baffles per unit length, m^{-1}
n_i	Number of bubbles, dimensionless
n_p	Number of points, dimensionless
C_D	Orifice discharge coefficient, dimensionless
x_0	Oscillation amplitude, m
f	Oscillation frequency, Hz

R_t	Radius of curvature of constriction centre, m
R_c	Radius of curvature of the sidewall of the convergent subsection, m
r	Radius of the bubbles, m
R_d	Radius of the sidewall of the divergent subsection, m
d_{32}	Sauter mean diameter, m
a	Specific interfacial area, m^{-1}
L_2	Straight tube length, m
u_g	Superficial gas velocity, m s^{-1}
t	Time, s
B	Time at end of a bubble, s
A	Time of arrival of bubble, s
T_G	Time spent within the bubble, s
T_M	time to transition from liquid to gas phase, s
V	Volume of reactor, m^3
$k_L a$	Volumetric liquid-side mass transfer coefficient, s^{-1}

Greek letters

ω	Angular frequency of oscillation, Hz
α	Baffle cross-sectional area, dimensionless
ρ	Density of the liquid, kg m^{-3}
μ	Dynamic viscosity, kg m^{-1} s^{-1}
ε_G	Gas holdup, dimensionless
ν	Kinematic viscosity, m^2 s^{-1}
σ	Surface tension, mN m^{-1}

Dimensionless numbers

Re_o	Oscillatory Reynolds number, dimensionless
St	Strouhal number, dimensionless

References

Ahmed, S.M.R., Phan, A., Harvey, A., 2018. Mass transfer enhancement as a function of oscillatory baffled reactor design. Chem. Eng. Process. Process Intensif. 130, 229–239. https://doi.org/10.1016/j.cep.2018.06.016

Ahmed, S.M.R., Phan, A.N., Harvey, A.P., 2019. Scale-Up of Gas–Liquid Mass Transfer in Oscillatory Multiorifice Baffled Reactors (OMBRs). Ind. Eng. Chem. Res. 58, 5929–5935. https://doi.org/10.1021/acs.iecr.8b04883

Al Ezzi, A.A.R., Najmuldeena, G., 2014. Gas Hold-Up, Mixing Time and Circulation Time in Internal Loop Airlift Bubble Column. J. Eng. Res. Appl. 4, 286–294.

Albijanić, B., Havran, V., Petrović, D.L., Đurić, M., Tekić, M.N., 2007. Hydrodynamics and mass transfer in a draft tube airlift reactor with dilute alcohol solutions. AIChE J. 53, 2897–2904. https://doi.org/10.1002/aic.11306

Almeida, F., Rocha, F., Ferreira, A., 2018. Analysis of Liquid Flow and Mixing in an Oscillatory Flow Reactor Provided with 2D Smooth Periodic Constrictions. U.Porto J. Eng. 4, 1–15. https://doi.org/10.24840/2183-6493_004.002_0001

Almeida, F., Rocha, F., Teixeira, J.A., Ferreira, A., 2022. The influence of electrolytes in aqueous solutions on gas-liquid mass transfer in an oscillatory flow reactor. Chem. Eng. Sci. 263, 118048–118066. https://doi.org/10.1016/j.ces.2022.118048

Alves, S.S., Orvalho, S.P., Vasconcelos, J.M.T., 2005. Effect of bubble contamination on rise velocity and mass transfer. Chem. Eng. Sci. 60, 1–9. https://doi.org/10.1016/j.ces.2004.07.053

Basařová, P., Pišlová, J., Mills, J., Orvalho, S., 2018. Influence of molecular structure of alcohol-water mixtures on bubble behaviour and bubble surface mobility. Chem. Eng. Sci. 192, 74–84. https://doi.org/10.1016/j.ces.2018.07.008

Baz-Rodríguez, S.A., Botello-Alvarez, J.E., Estrada-Baltazar, A., Vilchiz-Bravo, L.E., Padilla-Medina, J.A., Miranda-López, R., 2014. Effect of electrolytes in aqueous solutions on oxygen transfer in gas–liquid bubble columns. Chem. Eng. Res. Des. 92, 2352–2360. https://doi.org/10.1016/j.cherd.2014.02.023

Besagni, G., Brazzale, P., Fiocca, A., Inzoli, F., 2016. Estimation of bubble size distributions and shapes in two-phase bubble column using image analysis and optical probes. Flow Meas. Instrum. 52, 190–207. https://doi.org/10.1016/j.flowmeasinst.2016.10.008

Besagni, G., Inzoli, F., 2019. Bubble sizes and shapes in a counter-current bubble column with pure and binary liquid phases. Flow Meas. Instrum. 67, 55–82. https://doi.org/10.1016/j.flowmeasinst.2019.04.008

Besagni, G., Inzoli, F., Guido, G. De, Pellegrini, L.A., 2017. The dual effect of viscosity on bubble column hydrodynamics. Chem. Eng. Sci. 158, 509–538. https://doi.org/10.1016/j.ces.2016.11.003

Chaumat, H., Billet, A.M., Delmas, H., 2007. Hydrodynamics and mass transfer coefficient in bubble columns: influence of liquid phase surface tension. Chem. Eng. Sci. 62, 7378–7390. https://doi.org/10.1016/j.ces.2007.08.077

Chisti, Y., Kasper, M., Moo-Young, M., 1990. Mass transfer in external-loop airlift bioreactors using static mixers. Can. J. Chem. Eng. 68, 45–50. https://doi.org/10.1002/cjce.5450680106

Cruz, P., Rocha, F., Ferreira, A., 2021a. Crystallization of paracetamol from aqueous solutions in a planar oscillatory flow crystallizer: effect of the oscillation conditions on the nucleation kinetics. CrystEngComm 23, 6930–6941. https://doi.org/10.1039/D1CE00922B

Cruz, P., Rocha, F., Ferreira, A., 2021b. Crystallization of paracetamol from mixtures of ethanol and water in a planar oscillatory flow crystallizer: effect of the oscillation conditions on the crystal growth kinetics. CrystEngComm 23, 8301–8314. https://doi.org/10.1039/D1CE00858G

Cruz, P., Silva, C., Rocha, F., Ferreira, A., 2019. The axial dispersion of liquid solutions and solid suspensions in planar oscillatory flow crystallizers. AIChE J. 65, 16683. https://doi.org/10.1002/aic.16683

Cruz, P.C., Silva, C.R., Rocha, F.A., Ferreira, A.M., 2021. Mixing Performance of Planar Oscillatory Flow Reactors with Liquid Solutions and Solid Suspensions. Ind. Eng. Chem. Res. 60, 2663–2676. https://doi.org/10.1021/acs.iecr.0c04991

ElAzher, N., Gourich, B., Vial, C., Bellhaj, M.S., Bouzidi, A., Barkaoui, M., Ziyad, M., 2005. Influence of alcohol addition on gas hold-up, liquid circulation velocity and mass transfer coefficient in a split-rectangular airlift bioreactor. Biochem. Eng. J. 23, 161–167. https://doi.org/10.1016/j.bej.2004.12.003

Ferreira, A., Adesite, P.O., Teixeira, J.A., Rocha, F., 2017. Effect of solids on O2 mass transfer in an oscillatory flow reactor provided with smooth periodic constrictions. Chem. Eng. Sci. 170, 400–409. https://doi.org/10.1016/j.ces.2016.12.067

Ferreira, A., Pereira, G., Teixeira, J.A., Rocha, F., 2012. Statistical tool combined with image analysis to characterize hydrodynamics and mass transfer in a bubble column. Chem. Eng.

J. 180, 216–228. https://doi.org/10.1016/j.cej.2011.09.117

Ferreira, António, Rocha, F., Teixeira, J.A., Vicente, A., 2015. Apparatus for mixing improvement based on oscillatory flow reactors provided with smooth periodic constrictions. WO/2015/056156.

Ferreira, A, Teixeira, J.A., Rocha, F., 2015. O2 mass transfer in an oscillatory flow reactor provided with smooth periodic constrictions. Individual characterization of kL and a. Chem. Eng. J. 262, 499–508. https://doi.org/10.1016/j.cej.2014.09.125

Freitas, C., Teixeira, J.A., 2001. Oxygen mass transfer in a high solids loading three-phase internal-loop airlift reactor. Chem. Eng. J. 84, 57–61. https://doi.org/4-6

Freitas, C., Teixeira, J.A., 1998. Effect of liquid-phase surface tension on hydrodynamics of a three-phase airlift reactor with an enlarged degassing zone. Bioprocess Biosyst. Eng. 19, 451–457.

Gonçalves, A.L., Almeida, F., Rocha, F.A., Ferreira, A., 2021. Improving CO2 mass transfer in microalgal cultures using an oscillatory flow reactor with smooth periodic constrictions. J. Environ. Chem. Eng. 9, 106505–106517. https://doi.org/10.1016/j.jece.2021.106505

Hebrard, G., Zeng, J., Loubiere, K., 2009. Effect of surfactants on liquid side mass transfer coefficients: A new insight. Chem. Eng. J. 148, 132–138. https://doi.org/10.1016/j.cej.2008.08.027

Hur, Y.G., Yang, J.H., Jung, H., Lee, K.Y., 2014. Continuous alcohol addition in vaporized form and its effect on bubble behavior in a bubble column. Chem. Eng. Res. Des. 92, 804–811. https://doi.org/10.1016/j.cherd.2013.08.006

J.Zahradník, Fialová, M., Růžička, M., Drahoš, J., Kaštánek, F., Thomas, N.H., 1997. Duality of the gas-liquid flow regimes in bubble column reactors. Chem. Eng. Sci. 52, 3811–2826. https://doi.org/10.1016/S0009-2509(97)00226-1

Krishna, R., Urseanu, M.I., Dreher, A.J., 2000. Gas hold-up in bubble columns: influence of alcohol addition versus operation at elevated pressures. Chem. Eng. Process. Process Intensif. 39, 371–378. https://doi.org/10.1016/S0255-2701(00)00093-3

Llewellin, E.W., Del Bello, E., Taddeucci, J., Scarlato, P., Lane, S.J., 2012. The thickness of the falling film of liquid around a Taylor bubble, in: Proceedings of the Royal Society A: Mathematical, Physical and Engineering Sciences. pp. 1041–1064.

https://doi.org/10.1098/rspa.2011.0476

Luo, L., Yuan, J., Xie, P., Sun, J., Guo, W., 2013. Hydrodynamics and mass transfer characteristics in an internal loop airlift reactor with sieve plates. Chem. Eng. Res. Des. 91, 2377–2388. https://doi.org/10.1016/j.cherd.2013.06.002

Maceiras, R., Álvarez, E., Cancela, M.A., 2010. Experimental interfacial area measurements in a bubble column. Chem. Eng. J. 163, 331–336. https://doi.org/10.1016/j.cej.2010.08.011

Martin, M., Montes, F.J., Galán, M.A., 2007. Oxygen transfer from growing bubbles : Effect of the physical properties of the liquid. Chem. Eng. J. 128, 21–32. https://doi.org/10.1016/j.cej.2006.10.004

Mena, P., Ferreira, A., Teixeira, J.A., Rocha, F., 2011. Effect of some solid properties on gas – liquid mass transfer in a bubble column. Chem. Eng. Process. Process Intensif. 50, 181–188. https://doi.org/10.1016/j.cep.2010.12.013

Mena, P.C., Rocha, F.A., Teixeira, J.A., Sechet, P., Cartellier, A., 2008. Measurement of gas phase characteristics using a monofibre optical probe in a three-phase flow. Chem. Eng. Sci. 63, 4100–4115. https://doi.org/10.1016/j.ces.2008.05.010

Molina, E., Contreras, A., Chisti, Y., 1999. Gas holdup, liquid circulation and mixing behavior of viscous Newtonian media in a split-cylinder airlift bioreactor. Food Bioprod. Process. 77, 27–32. https://doi.org/10.1205/096030899532222

Montgomery, D.C., 2000. Design and Analysis of Experiments, 5th ed. John Wiley & Sons, Inc., New York.

Moraveji, M.K., Fakhari, M.E., Mohsenzadeh, E., Davarnejad, R., 2012. Hydrodynamics and oxygen mass transfer in a packed bed split-cylinder airlift reactor containing dilute alcoholic solutions. Heat Mass Transf. 49, 11–19. https://doi.org/10.1007/s00231-012-1056-0

Moraveji, M.K., Sajjadi, B., Davarnejad, R., 2011. Gas-Liquid Hydrodynamics and Mass Transfer in Aqueous Alcohol Solutions in a Split-Cylinder Airlift Reactor. Chem. Eng. Technol. 34, 465–474. https://doi.org/10.1002/ceat.201000373

Mouza, A.A., Dalakoglou, G.K., Paras, S.V., 2005. Effect of liquid properties on the performance of bubble column reactors with fine pore spargers. Chem. Eng. Sci. 60, 1465–1475. https://doi.org/10.1016/j.ces.2004.10.013

Ni, X., Oliveira, M., 2004. Characterization of a Gas-Liquid OBC: Bubble Size and Gas Holdup. AIChE J. 50, 3019–3033. https://doi.org/10.1002/aic.10282

Oliveira, M., Ni, X., 2004. Effect of hydrodynamics on mass transfer in a gas – liquid oscillatory baffled column. Chem. Eng. J. 99, 59–68. https://doi.org/10.1016/j.cej.2004.01.002

Oliveira, M., Ni, X., 2001. Gas hold-up and bubble diameters in a gassed oscillatory baffled column. Chem. Eng. Sci. 56, 6143–6148. https://doi.org/10.1016/S0009-2509(01)00257-3

Onken, U., Weiland, P., 1980. Hydrodynamics and Mass Transfer in an Airlift Loop Fermenter. Eur. J. Appl. Microbiol. Biotechnol. 10, 31–40.

Pereira, F.M., Sousa, D.Z., Alves, M.M., Mackley, M.R., Reis, N.M., 2014. CO_2 dissolution and design aspects of a multiorifice oscillatory baffled column. Ind. Eng. Chem. Res. 53, 17303–17316. https://doi.org/10.1021/ie403348g

Philip, J., Proctor, J.M., Niranjan, K., Davidson, J.F., 1990. Gas hold-up and liquid circulation in internal loop reactors containing highly viscous newtonian and non-newtonian liquids. Chem. Eng. Sci. 45, 651–664. https://doi.org/10.1016/0009-2509(90)87008-G

Ramezani, M., Legg, M.J., Haghighat, A., Li, Z., Vigil, R.D., Olsen, M.G., 2017. Experimental investigation of the effect of ethyl alcohol surfactant on oxygen mass transfer and bubble size distribution in an air-water multiphase Taylor-Couette vortex bioreactor. Chem. Eng. J. 319, 288–296. https://doi.org/10.1016/j.cej.2017.03.005

Reis, N., Mena, P.C., Vicente, A.A., Teixeira, J.A., Rocha, F.A., 2007. The intensification of gas-liquid flows with a periodic, constricted oscillatory-meso tube. Chem. Eng. Sci. 62, 7454–7462. https://doi.org/10.1016/j.ces.2007.09.018

Reis, N., Pereira, R.N., Vicente, A.A., Teixeira, J.A., 2008. Enhanced gas-liquid mass transfer of an oscillatory constricted-tubular reactor. Ind. Eng. Chem. Res. 47, 7190–7201. https://doi.org/10.1021/ie8001588

Snape, J.B., Fialova, M., Zahradnik, J., Thomas, N.H., 1992. Hydrodynamic studies in an external loop airlift reactor containing aqueous electrolyte and sugar solutions. Chem. Eng. Sci. 47, 3387–3394. https://doi.org/10.1016/0009-2509(92)85049-H

Yang, H., Chen, A., Geng, S., Cheng, J., Gao, F., Huang, Q., Yang, C., 2022. Influences of fluid physical properties, solid particles, and operating conditions on the hydrodynamics in

slurry reactors. Chinese J. Chem. Eng. 44, 51–71. https://doi.org/10.1016/j.cjche.2021.03.045

Yang, J.H., Yang, J.-I., Kim, H.-J., Chun, D.H., Lee, H.-T., Jung, H., 2010. Two regime transitions to pseudo-homogeneous and heterogeneous bubble flow for various liquid viscosities. Chem. Eng. Process. Process Intensif. 49, 1044–1050. https://doi.org/10.1016/j.cep.2010.07.015

List of Tables

Table 1. Operating conditions

f (Hz)	1; 2; 3; 4
x_o (mm)	4; 9; 19
Q (ml min^{-1})	5; 10; 20; 60; 100
vvm (min^{-1})	1.43; 0.86; 0.29; 0.14; 0.07
u_g (mm s^{-1})	9.8; 5.9; 2.0; 0.98; 0.49
St	0.29; 0.13; 0.062
Re_o (ethanol)	270; 541; 811; 1082; 609; 1218; 1826; 2435; 1285; 2570; 3855; 5140
Re_o (sucrose)	66; 133; 199; 265 149; 298; 448; 597; 315; 630; 945; 1260

Table 2. Liquid properties of the solutions (Ferreira et al., 2012).

Solutions	Surface tension (mN/m)	Viscosity (cP)
Water	73.1	1
Ethanol (6.31 % (w/v)) (1.37 M)	53	1.23
Sucrose (48.3 % (w/v)) (1.41 M)	73.3	3.33

Table 3. Comparison between experimental $k_L a$, ε_G, d_{32}, k_L and a values obtained in this study with the ones reported in literature for different common gas-liquid contactors using ethanol and sucrose aqueous solutions.

Gas-liquid contactor	Gas input	Oscillatory conditions	Compound concentration (M)	$k_L a$ (h^{-1})	ε_G	d_{32} (mm)	k_L ($m\ h^{-1}$)	a (m^{-1})	Reference
Airlift reactor[2]	10 mm s^{-1}	Without oscillation	0.21 ethanol	43	_____	_____	_____	_____	(Albijanić et al., 2007)
Bubble column[1]	3.7-18.8 mm s^{-1}	Without oscillation	0.01 ethanol	_____	_____	6-15	_____	_____	(Besagni and Inzoli, 2019)
Bubble column[1]	0.5-1.0 mm s^{-1}	Without oscillation	0.2 butanol	_____	0.007-0.12	1.1-1.3	_____	38-554	(Mouza et al., 2005)
Taylor-Couette vortex bioreactor	400 cm^3 min^{-1}	0 rpm 400 rpm	1.1 ethanol	9 27	_____	4 3.5	_____	_____	(Ramezani et al., 2017)
Airlift reactor[2]	10 mm s^{-1}	Without oscillation	0.83 sucrose 1.1 sucrose	_____	0.018 0.011	_____	_____	_____	(Molina et al., 1999)
Bubble column[1]	20 mm s^{-1}		2.1 ethanol	_____	0.07	_____	_____	_____	(Al Ezzi and Najmuldeena, 2014)
Split-cylinder airlift reactor[2]	10 mm s^{-1}	Without oscillation	0.1 ethanol 0.2 ethanol	59 68	0.031 0.045	1.1 0.85	0.3 0.2	197 340	(Moraveji et al., 2011)
Split-rectangular airlift reactor[2]	20 mm s^{-1}	Without oscillation	0.01 propanol	36	0.025	____	____	____	(ElAzher et al., 2005)
Airlift reactor[2]	12 mm	Without oscillation	1.5 sucrose 0.14 2-	9	0.029	____	____	____	(Onken and Weiland,

	s^{-1}		propanol	64	0.026				1980)
Airlift reactor[2]									(Freitas and Teixeira, 2001, 1998)
	10 mm s^{-1}	Without oscillation	0.22 ethanol	4	0.008	____	____	____	
Bubble column[1]	2-10 mm s^{-1}	Without oscillation	1.37 ethanol	25-113	0.013-0.063	3.8-5.0	1.2-1.6	20-75	(Ferreira et al., 2012)
			1.41 sucrose	7-36	0.019-0.085	4.6-6.0	0.36-0.43	25-85	
Packed bed split cylinder airlift reactor[2]	2-10 mm s^{-1}	Without oscillation	0.22 ethanol packed	21-72	0.02-0.085	0.6-0.7	0.096-0.1	210-750	(Moraveji et al., 2012)
			0.22 ethanol unpacked	18-65	0.01-0.05	0.4-0.8	0.12-0.16	150-400	
Oscillatory flow reactor provided with smooth periodic constrictions (OFR-SPC)*	0.5-10 mm s^{-1}	$x_0 = 4$ mm $f = 1$ Hz	1.37 ethanol	28-126	0.004-0.07	0.8-3.3	0.9-1.0	31-127	Present study
			1.41 sucrose	13-61	0.004-0.067	1.4-6.3	0.76-0.95	17-64	
Oscillatory flow reactor provided with smooth periodic constrictions (OFR-SPC)*	0.5-10 mm s^{-1}	$x_0 = 19$ mm $f = 2$ Hz	1.37 ethanol	39-384	0.005-0.06	1.1-2.0	1.5-2.2	26-176	Present study
			1.41 sucrose	18-185	0.005-0.057	1.4-2.1	0.82-1.1	22-166	

*Power density estimated in OFR-SPC (~105 W m^{-3}) for these oscillation conditions and $u_g = 10$ mm s^{-1}

[1]Power density estimated in bubble columns(~90 W m^{-3}) for $u_g = 10$ mm s^{-1}

[2]Power density estimated in airlift (20 to 60 W m^{-3}) for $u_g = 10$ mm s^{-1}

Figure captions

Fig. 1. Schematic representation of the oscillatory reactor. D – inner diameter of the straight section (16 mm); d_0 – internal tube diameter in the constrictions (~7 mm); L_1 – constriction length; L_2 – straight tube length ($L_1 + L_2 = 54$ mm); R_c – radius of curvature of the sidewall of the convergent subsection; R_d – radius of the sidewall of the divergent subsection; R_t – radius of curvature of constriction centre

Fig. 2. Image processing scheme (Ferreira et al., 2012)

Fig. 3. Typical shape of a conical probe signal. A – Time of arrival of bubble; B – Time at end of a bubble; C – Low threshold; D – High threshold; T_G - The time spent within a bubble; T_m – The time to transition from liquid to gas phase; V_G – Gas level voltage; V_L – Liquid level voltage; V_B – amplitude of the noise of the signal peak to peak.

Fig. 4. Cube plot of the experimental design

Fig. 5. Effect of oscillatory conditions, both x_0 f ranging from 4 to 19 mm and 1 to 4 Hz respectively on $k_L a$, under u_g ranging from 2 to 9.8 mm s^{-1}: A) Ethanol 6.31 % (w/v); B) Sucrose 48.3 % (w/v).

Fig. 6. Experimental and calculated $k_L a \times 10^3$: A) from equation (14); B) from equation (15). Error bars correspond to 95 % confidence interval.

Fig. 7. Effect of oscillatory conditions on ε_G for ethanol ($f = 1$ Hz - ●, $f = 2$ Hz - ■, $f = 3$ Hz - ▲, $f = 4$ Hz - ◆) and sucrose ($f = 1$ Hz - ○, $f = 2$ Hz - □, $f = 3$ Hz - △, $f = 4$ Hz - ◇) solutions, under constant u_g and f ranging from 0.49 to 9.8 mm s^{-1} and 1 to 4 Hz, respectively: A) St = 0.29 (Heterogeneous regime); B) St = 0.13 (transition regime at $f > 2$ Hz, $u_g > 6$ mm s^{-1}); C) St = 0.062 (Homogeneous regime).

Fig. 8. Bubble size distribution for $x_0 = 4$ mm, $u_G = 1.0$ mm s^{-1}.

Fig. 9. Effect of oscillatory conditions, both x_0 and f ranging from 4 to 19 mm and 1 to 4 Hz respectively on d_{32}, under u_g ranging from 0.49 to 9.8 mm s^{-1}: A) Ethanol 6.31 % (w/v); B) Sucrose 48.3 % (w/v).

Fig. 10. Effect of oscillatory conditions, under constant u_g from 0.49 to 9.8 mm s^{-1} on k_L ($x_0 = 4$ mm and $f = 1$ Hz - ●, $f = 2$ Hz - ■, $f = 3$ Hz - ◆, $f = 4$ Hz - ▲; $x_0 = 19$ mm and $f = 1$ Hz - ○, $f = 2$ Hz - □, $f = 3$ Hz - ◇, $f = 4$ Hz - △) and a ($x_0 = 4$ mm and $f = 1$ Hz - ●, $f = 2$ Hz - ■, $f = 3$ Hz - ◆, $f = 4$ Hz - ▲; $x_0 = 19$ mm and $f = 1$ Hz - ○, $f = 2$ Hz - □, $f = 3$ Hz - ◇, $f = 4$ Hz - △) for: A) ethanol; B) sucrose. Almeida et al. (2022) - (·····) for electrolytes. Error bars correspond to a 95 % confidence interval obtained for k_L and a.

Fig. 11. Effect of liquid properties for all operating conditions on: A) ε_G - ■, and d_{32} - ■; B) $k_L a$ - ■, k_L - ■, a - ■. Error bars correspond to 95 % confidence interval.

List of figures

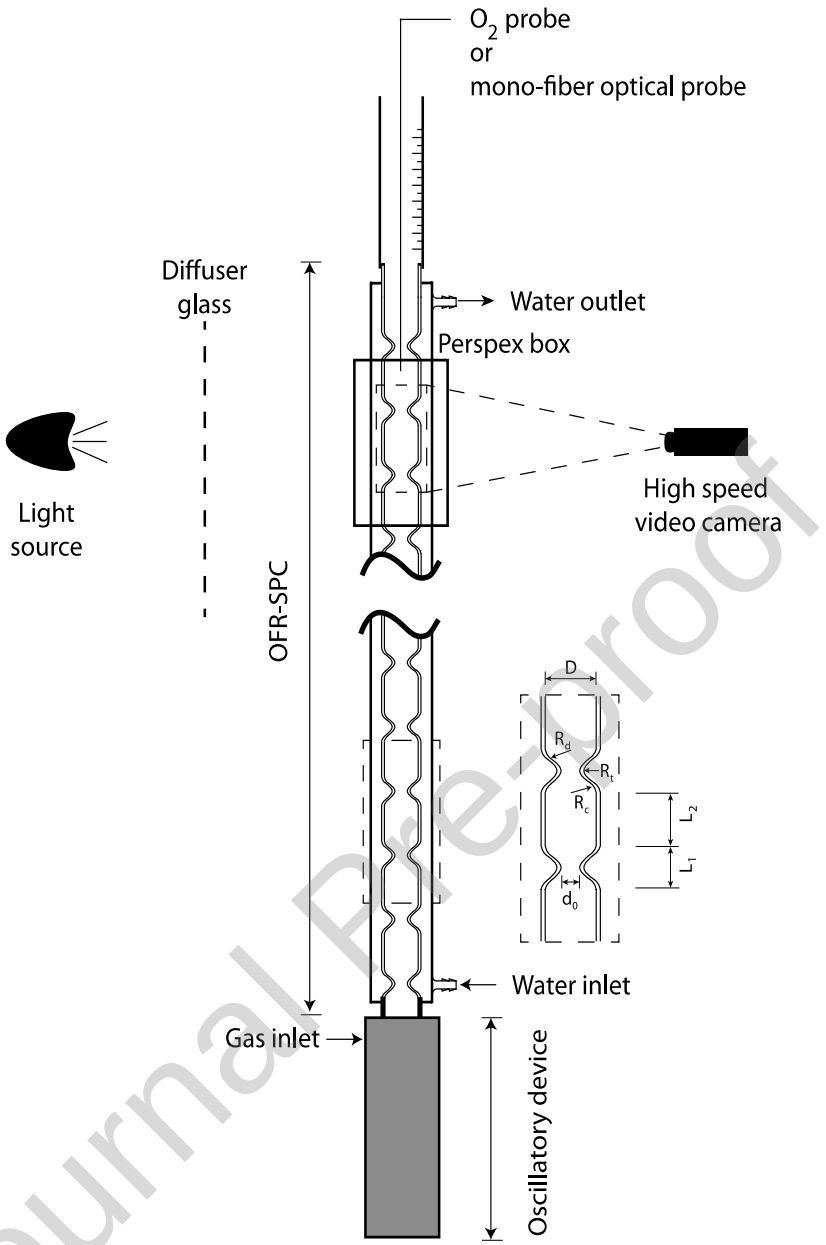

Fig. 1. Schematic representation of the oscillatory reactor. D – inner diameter of the straight section (16 mm); d_0 – internal tube diameter in the constrictions (~7 mm); L_1 – constriction length; L_2 – straight tube length ($L_1 + L_2 = 54$ mm); R_c – radius of curvature of the sidewall of the convergent subsection; R_d – radius of the sidewall of the divergent subsection; R_t – radius of curvature of constriction centre

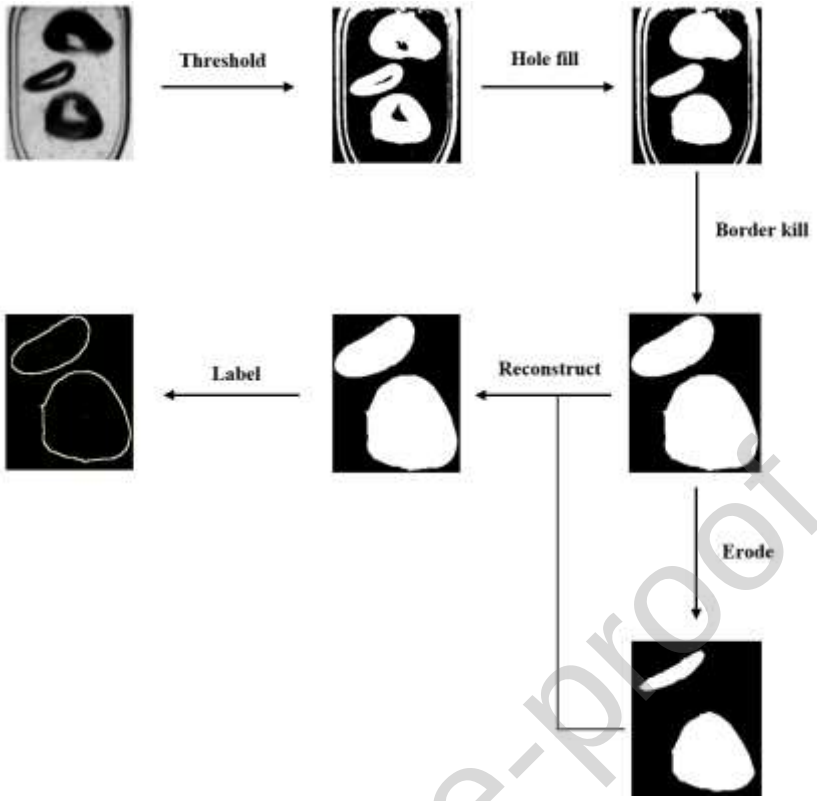

Fig. 2. Image processing scheme

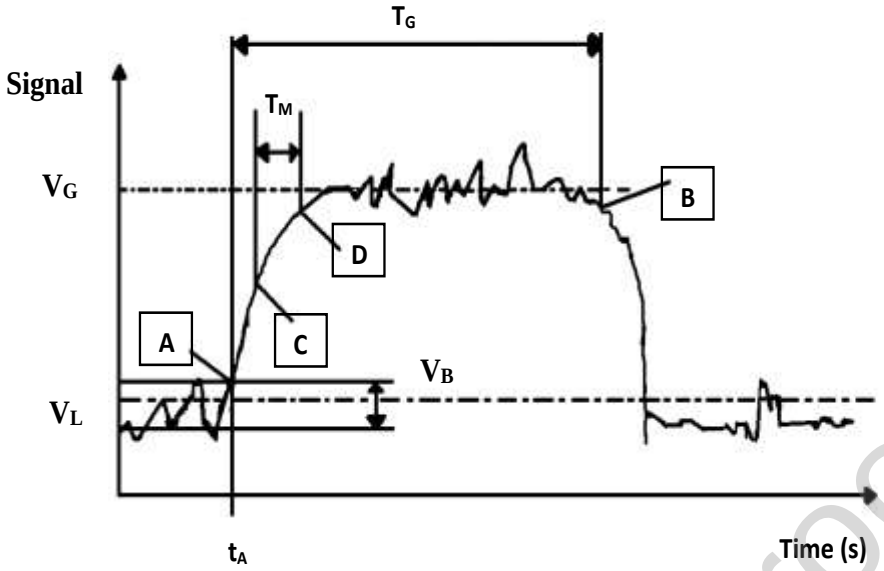

Fig. 3. Typical shape of a conical probe signal. A – Time of arrival of bubble; B – Time at end of a bubble; C – Low threshold; D – High threshold; T_G - The time spent within a bubble; T_m – The time to transition from liquid to gas phase; V_G – Gas level voltage; V_L – Liquid level voltage; V_B – amplitude of the noise of the signal peak to peak.

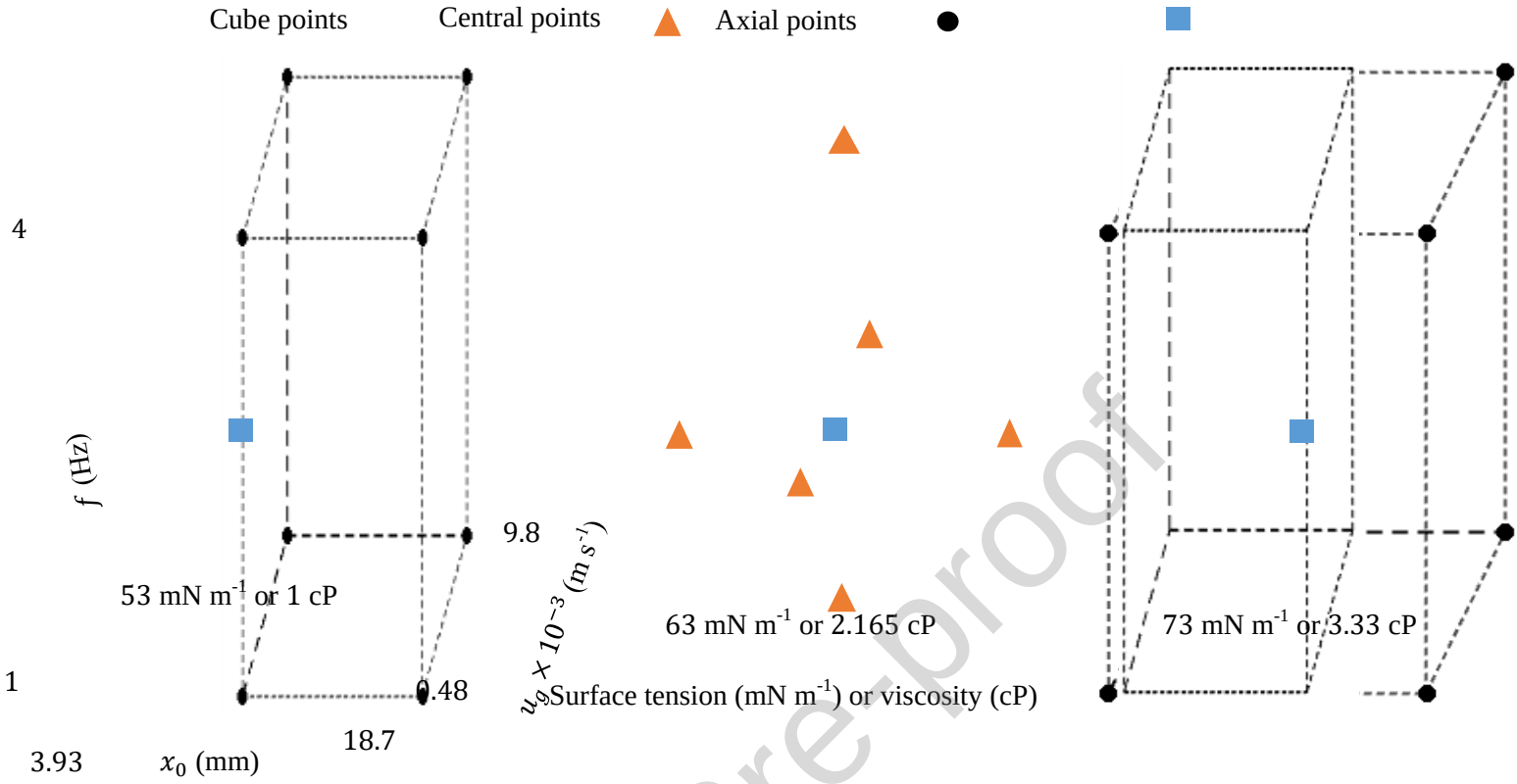

Fig. 4. Cube plot of the experimental design

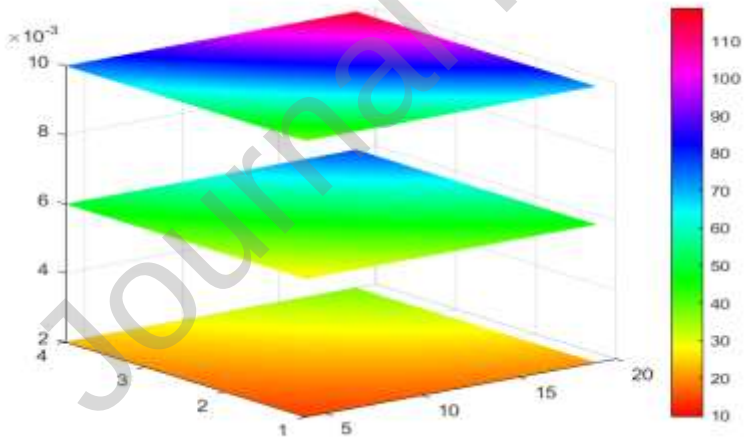

$k_L a \times 10^3$ (s^{-1})

A)

u_g ($m\ s^{-1}$)

f (Hz)

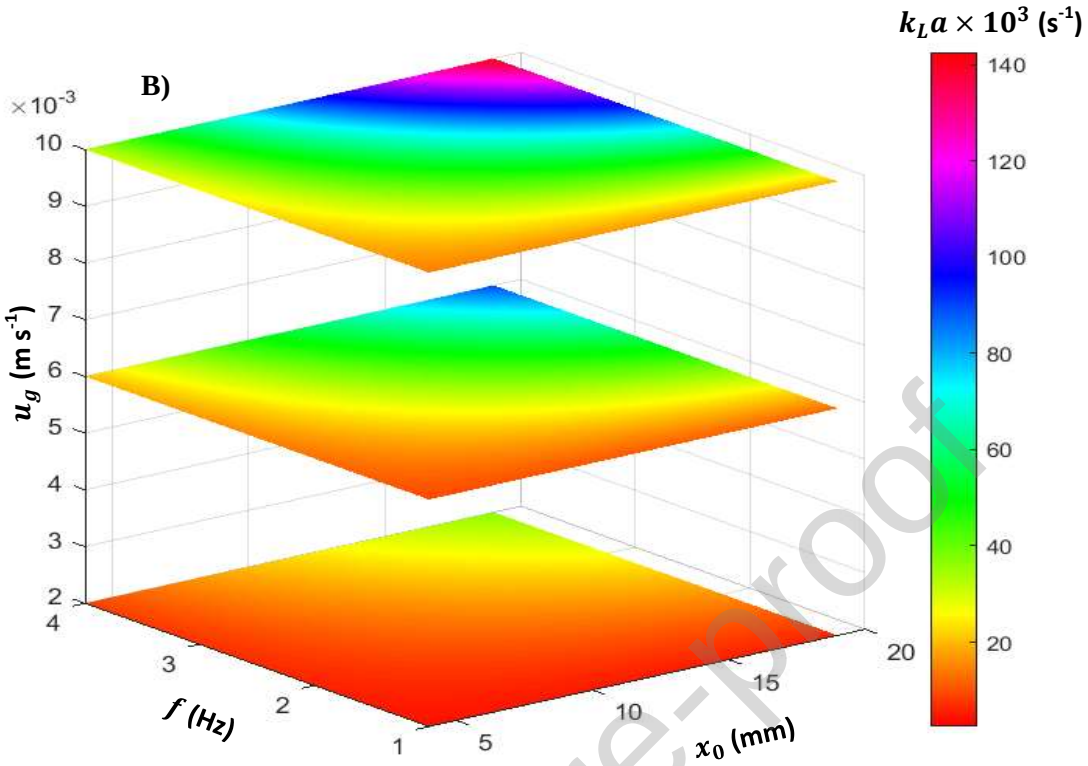

Fig. 5. Effect of oscillatory conditions, both x_0 and f ranging from 4 to 19 mm and 1 to 4 Hz respectively on $k_L a$, under u_g ranging from 2 to 9.8 mm s^{-1}: A) Ethanol 6.31 % (w/v); B) Sucrose 48.3 % (w/v).

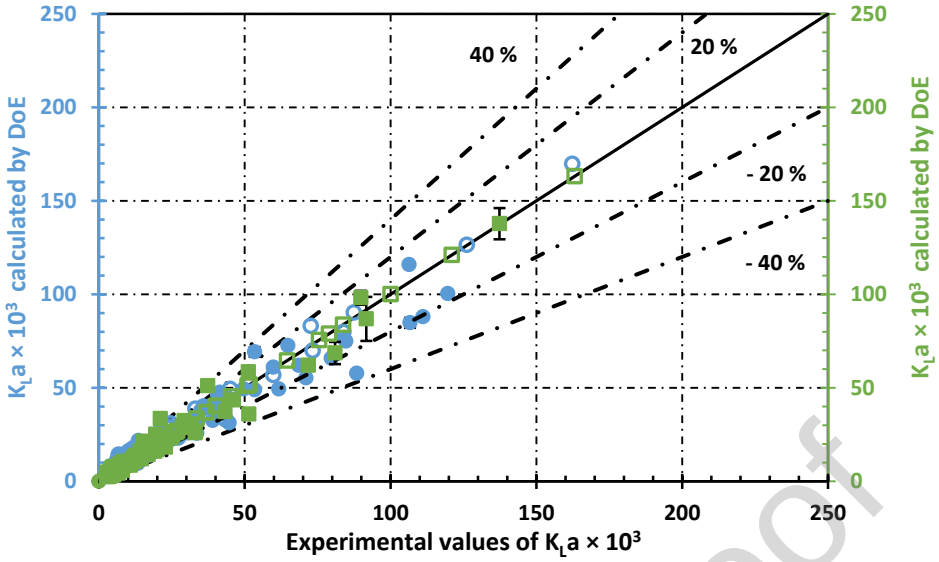

Fig. 6. Experimental and calculated $k_L a \times 10^3$ from equation (14): ● – ethanol, ○ – water; from equation (15): ■ – sucrose, □ – water. Error bars correspond to 95 % confidence interval.

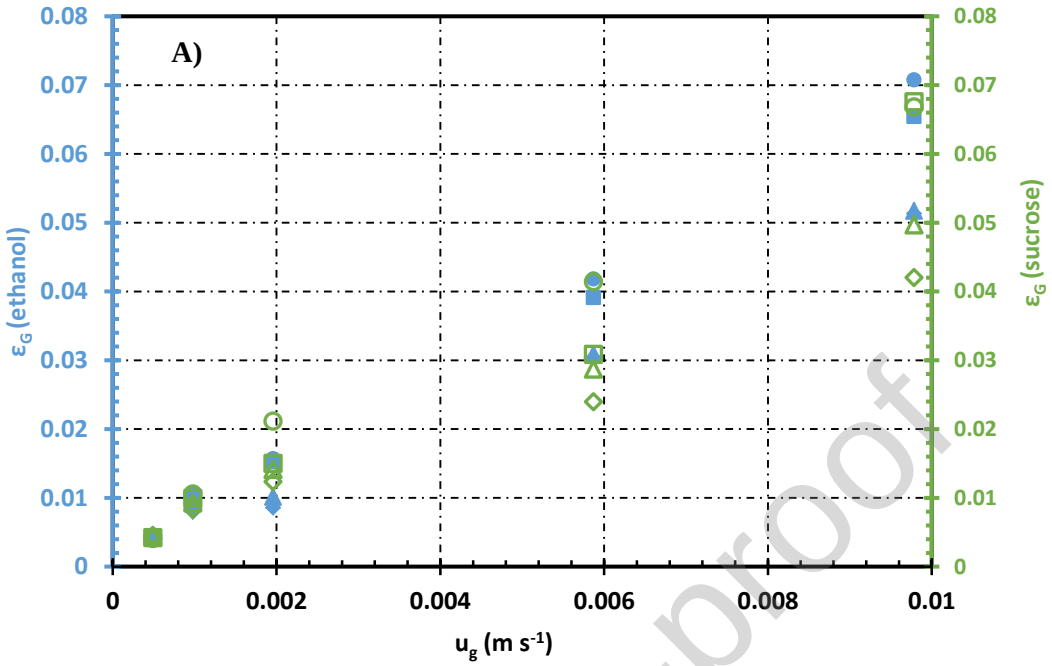

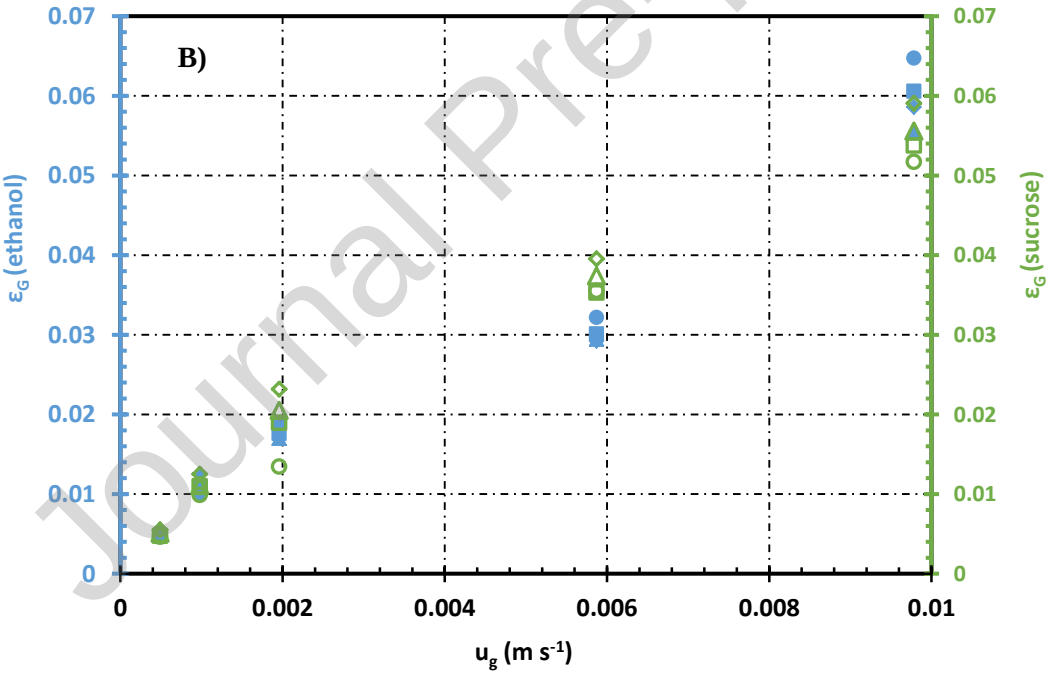

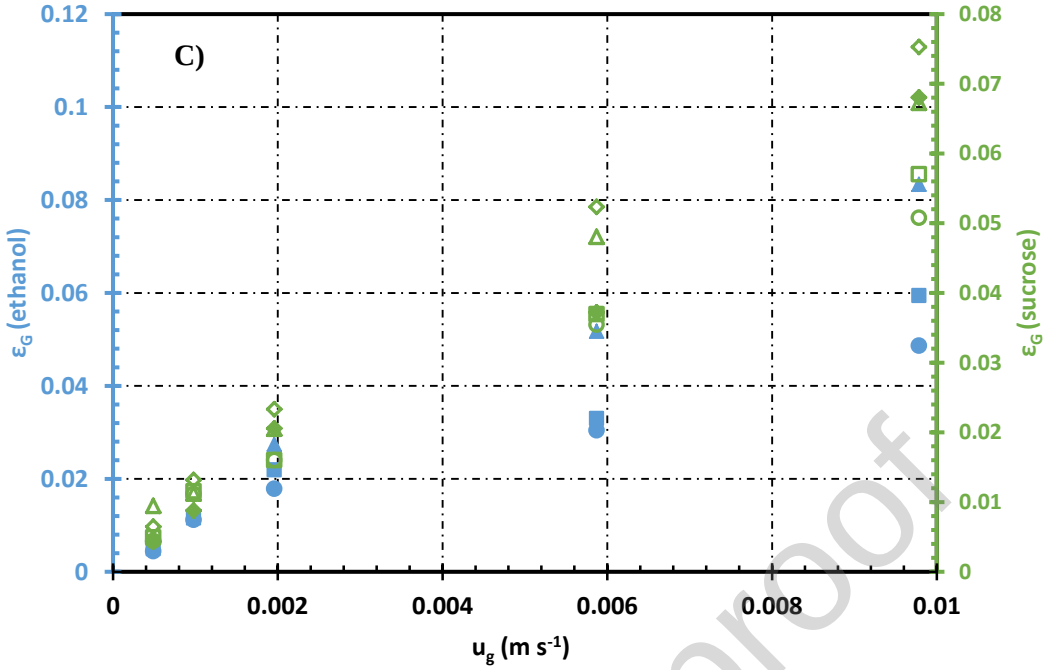

Fig. 7. Effect of oscillatory conditions on ε_G for ethanol (f = 1 Hz - ●, f = 2 Hz - ■, f = 3 Hz -▲, f = 4 Hz - ◆) and sucrose (f = 1 Hz - ○, f = 2 Hz - □, f = 3 Hz - △, f = 4 Hz - ◇) solutions, under constant u_g and f ranging from 0.49 to 9.8 mm s^{-1} and 1 to 4 Hz, respectively: A) St = 0.29 (Heterogeneous regime); B) St = 0.13 (transition regime at $f > 2$ Hz, $u_g > 6$ mm s^{-1}); C) St = 0.062 (Homogeneous regime).

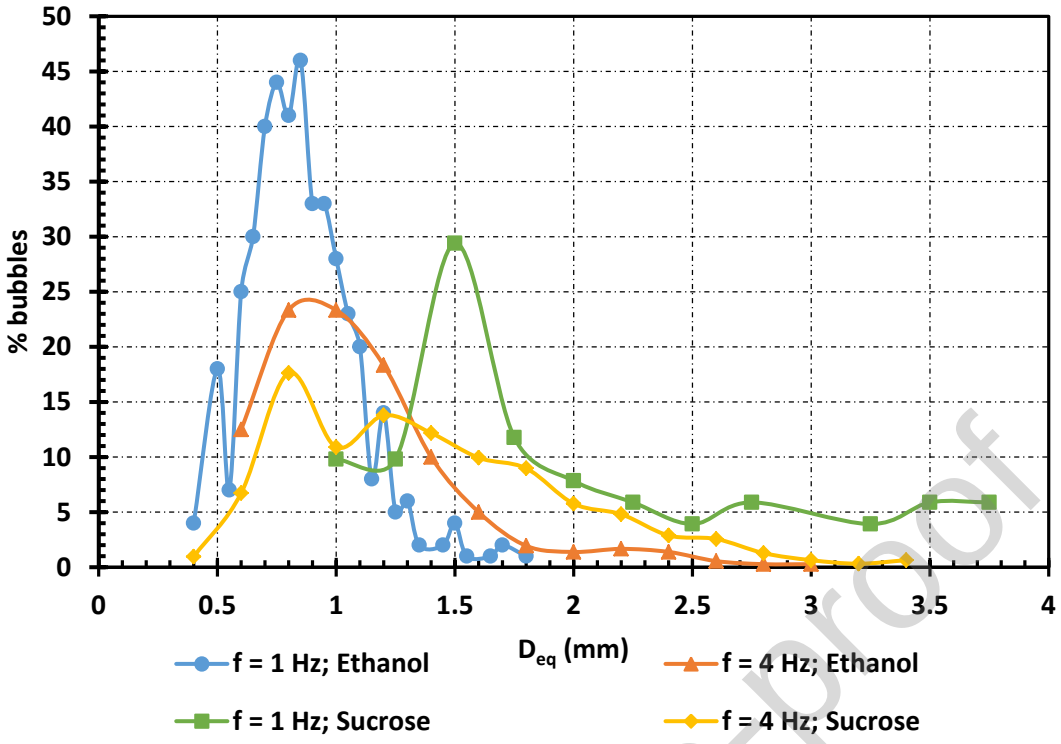

Fig. 8. Bubble size distribution for $x_0 = 4$ mm, $u_G = 1.0$ mm s^{-1}.

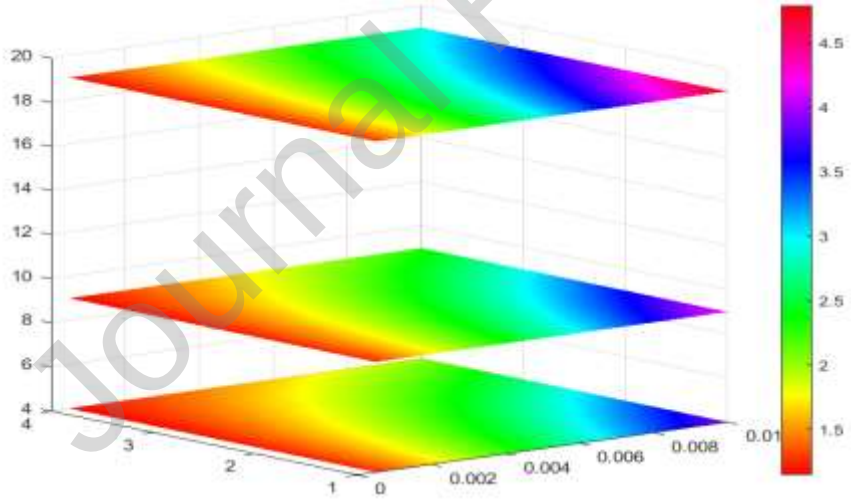

A)

x_0 (mm)

f (Hz)

u_g (m s^{-1})

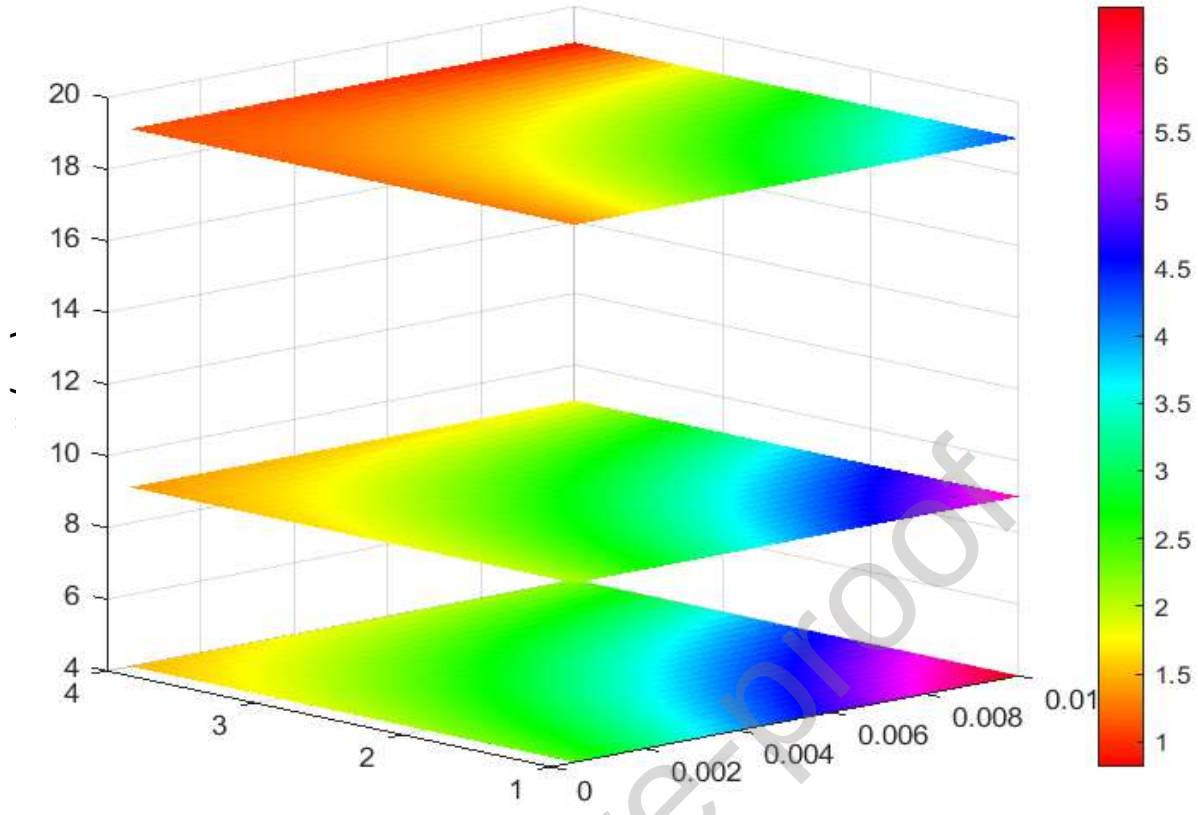

Fig. 9. Effect of oscillatory conditions, both x_0 and f ranging from 4 to 19 mm and 1 to 4 Hz respectively on d_{32}, under u_g ranging from 0.49 to 9.8 mm s^{-1}: A) Ethanol 6.31 % (w/v); B) Sucrose 48.3 % (w/v).

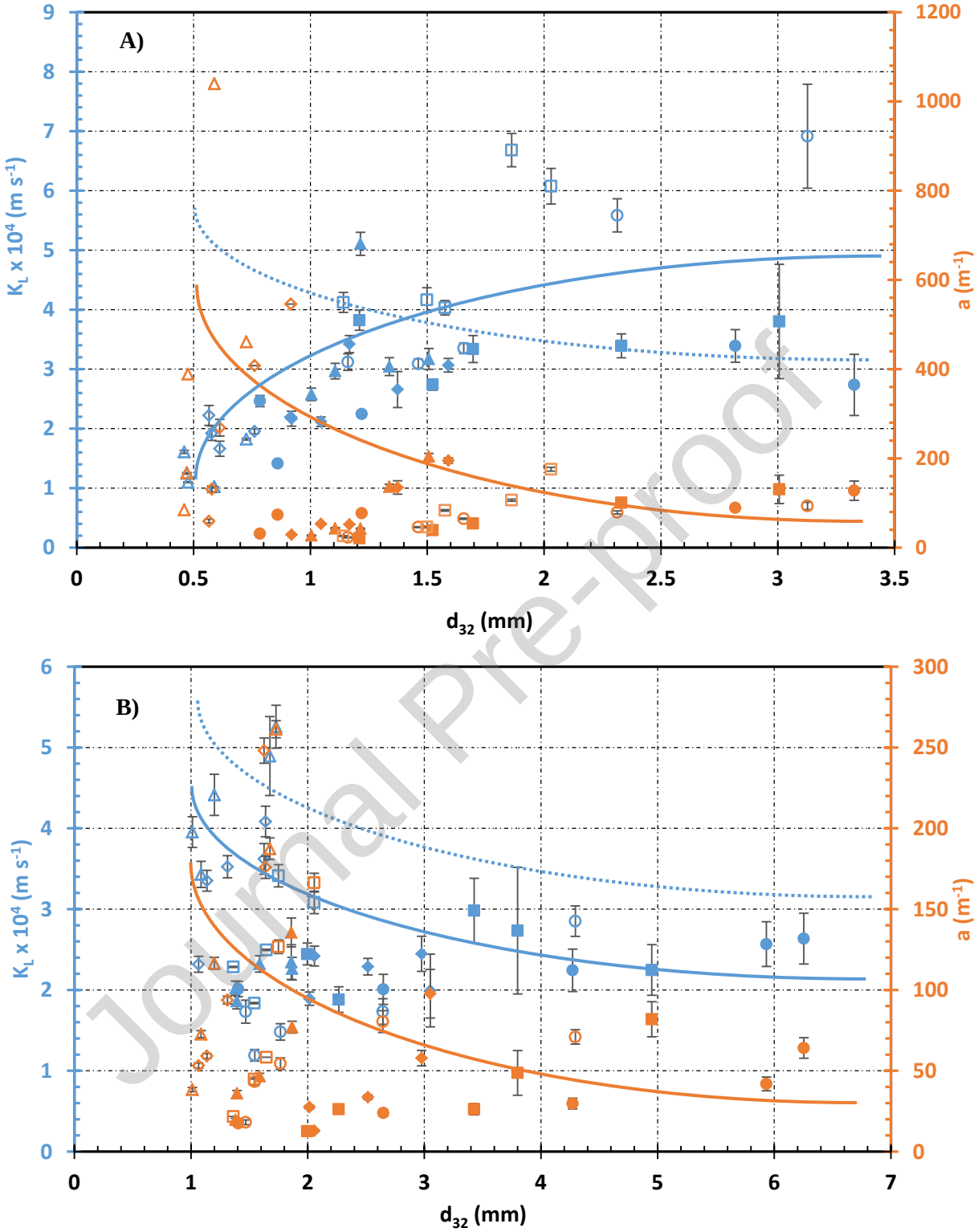

Fig. 10. Effect of oscillatory conditions, under constant u_g from 0.49 to 9.8 mm s^{-1} on k_L ($x_0 = 4$ mm and $f = 1$ Hz - ●, $f = 2$ Hz - ■, $f = 3$ Hz - ◆, $f = 4$ Hz - ▲; $x_0 = 19$ mm and $f = 1$ Hz - ○, $f = 2$ Hz - □, $f = 3$ Hz - ◇, $f = 4$ Hz - △) and a ($x_0 = 4$ mm and $f = 1$ Hz - ●, $f = 2$ Hz - ■, $f = 3$ Hz - ◆, $f = 4$ Hz - ▲; $x_0 = 19$ mm and $f = 1$ Hz - ○, $f = 2$ Hz - □, $f = 3$ Hz - ◇, $f = 4$ Hz - △) for: A) ethanol; B) sucrose. Almeida et al. (2022) - (·····) for electrolytes. Error bars correspond to 95 % confidence interval.

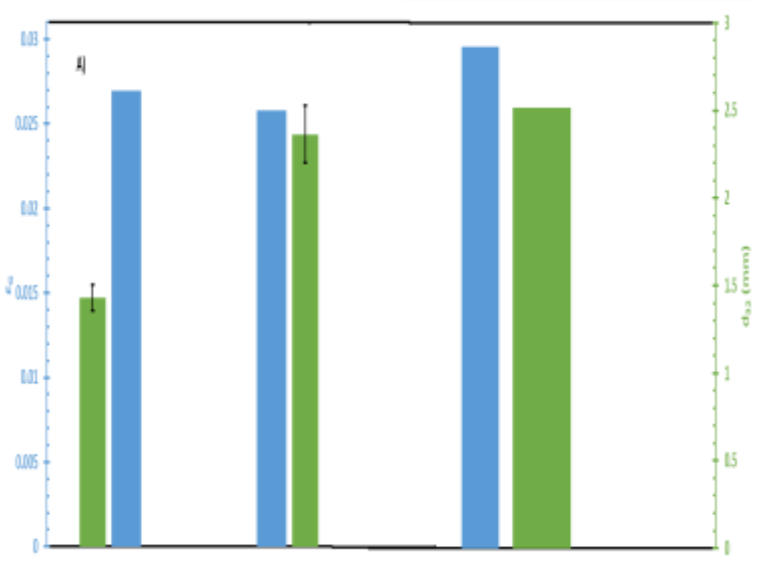

Ethanol (6.31 % (w/v)) **Sucrose 48.3 % (w/v)** **Water, Ferreira et al (2015)**

Fig. 11. Effect of liquid properties for all operating conditions on: A) ε_G - ■, and d_{32} - ■; B) $k_L a$ - ■, k_L - ■, and a - ■. Error bars correspond to 95 % confidence interval.

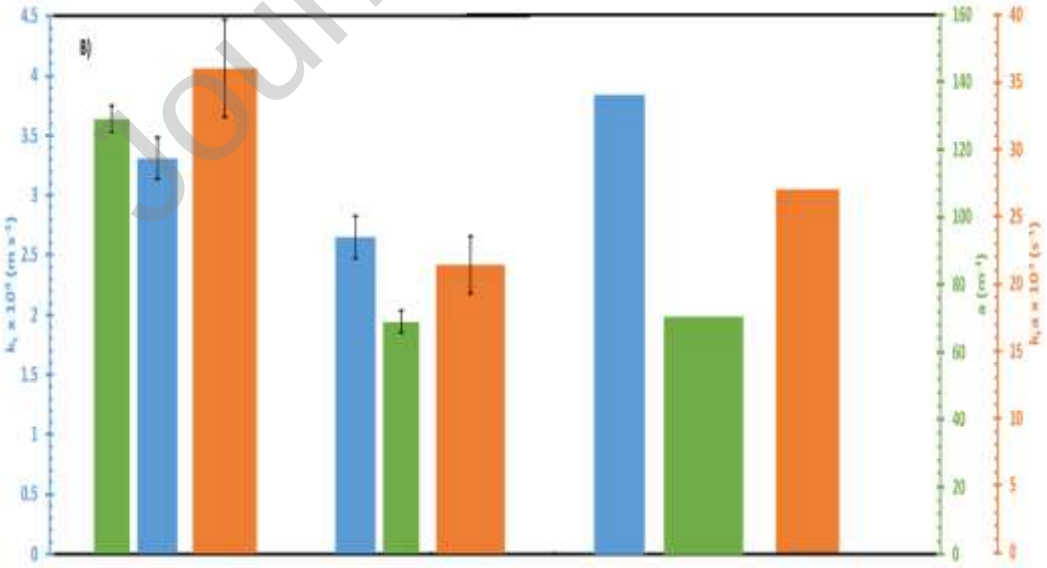

Declaration of interests

☒ The authors declare that they have no known competing financial interests or personal relationships that could have appeared to influence the work reported in this paper.

☐The authors declare the following financial interests/personal relationships which may be considered as potential competing interests:

Highlights

- Mass transfer in the OFR-SPC was higher than in the conventional gas-liquid contactors, with moderate power consumption.
- An increase in oscillatory conditions improves mass transfer.
- For viscous medium, an oscillation increase originates a modal BSD, compared to bubble column.
- Higher oscillations decrease k_L in the presence of ethanol, in opposite to sucrose solutions.
- The addition of ethanol or sucrose barely affected gas holdup in the OFR-SPC face to common gas-liquid contactors.